The Total Carbon Column Observing Network's GGG2014 Data Version

Debra Wunch[1], Geoffrey C. Toon[1,2], Vanessa Sherlock[3], Nicholas M. Deutscher[4], Cate Liu[1], Dietrich G. Feist[5], Paul O. Wennberg[1]

October 15, 2015

Abstract

This paper describes the updates to the Total Carbon Column Observing Network (TCCON) data analysis to generate the GGG2014 data version, which is a significant improvement over the GGG2012 data version. Laser sampling errors (a.k.a. "ghosts") have been corrected, improving the network-wide consistency in the retrieved column-averaged dry-air mole fractions. The *a priori* profiles used in the retrievals have been improved using airborne and balloon-borne *in situ* measurements. The spectroscopic linelists are improved for H_2O, CO, $^{13}CH_4$, and the solar Fraunhofer absorptions. We have updated the airmass-dependence corrections and scaling factors required to tie the TCCON to the currently-accepted World Meteological Organization gas standard scales. Finally, an error budget is presented. The GGG2014 TCCON data are available from the Carbon Dioxide Information Analysis Center (CDIAC) at `http://tccon.ornl.gov`.

[1] California Institute of Technology, Pasadena, CA, USA.
[2] Jet Propulsion Laboratory, California Institute of Technology, Pasadena, CA, USA.
[3] Wellington, New Zealand.
[4] University of Wollongong, Wollongong, Australia.
[5] Max Planck Institute for Biogeochemistry, Jena, Germany.

To cite this document, please use:
Wunch, D., G. C. Toon, V. Sherlock, N. M. Deutscher, X. Liu, D. G. Feist, and P. O. Wennberg. The Total Carbon Column Observing Network's GGG2014 Data Version. doi:10.14291/tccon.ggg2014.documentation.R0/1221662, 2015.

1 Introduction

The Total Carbon Column Observing Network (TCCON) provides atmospheric column-averaged dry-air mole fractions of CO_2, CH_4, CO, N_2O, H_2O, HDO, and HF to the scientific and satellite validation communities. These data have been used in scientific investigations of the carbon cycle [*Sussmann et al.*, 2012; *Keppel-Aleks et al.*, 2012, 2011; *Chevallier et al.*, 2011; *Guerlet et al.*, 2013; *Wunch et al.*, 2013; *Deutscher et al.*, 2014], development of improved spectroscopic models and line lists [*Thompson et al.*, 2012; *Scheepmaker et al.*, 2013; *Reuter et al.*, 2011; *Tran et al.*, 2010; *Tran and Hartmann*, 2008; *Reuter et al.*, 2012; *Miller and Wunch*, 2012; *Long and Hodges*, 2012; *Hartmann et al.*, 2009; *Gordon et al.*, 2011, 2010; *Galli et al.*, 2012], in the validation of satellite measurements and satellite algorithm development [*Morino et al.*, 2011; *Wunch et al.*, 2011a; *Butz et al.*, 2011; *Schneising et al.*, 2012; *Schepers et al.*, 2012; *Reuter et al.*,

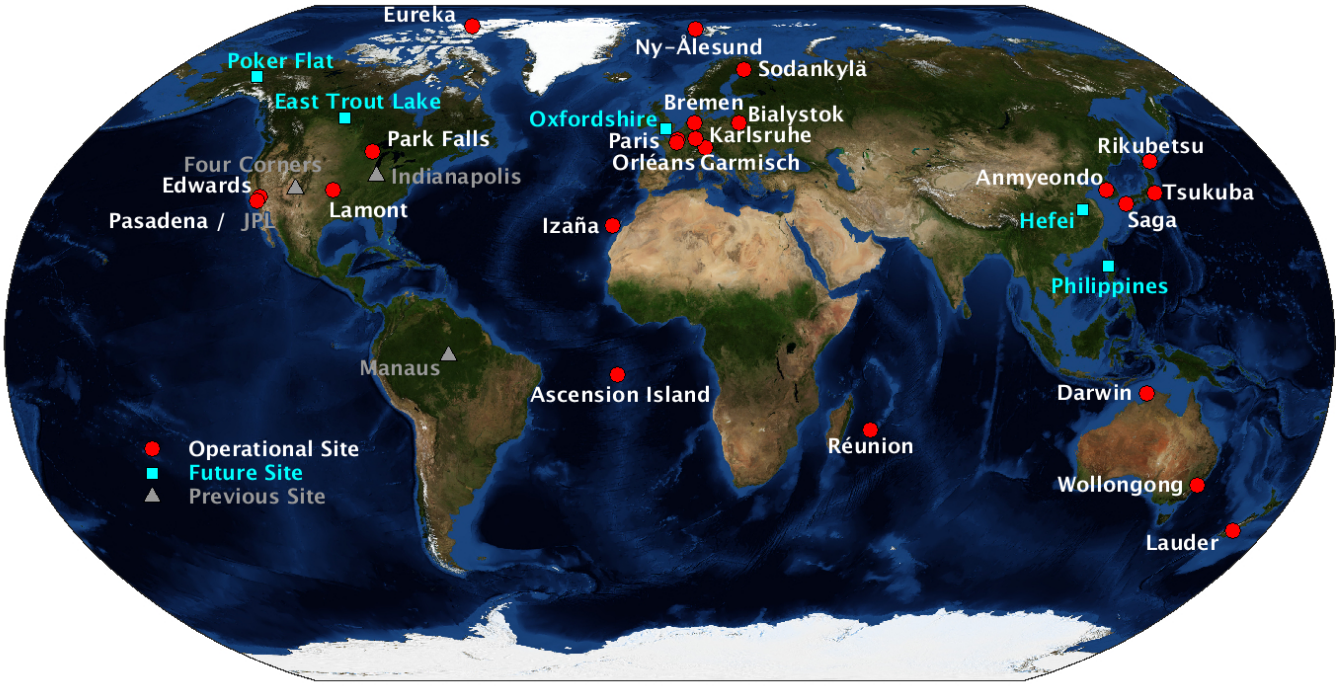

Figure 1: A map showing the locations of the TCCON stations. The background image is the Blue Marble: Next Generation, produced by Reto Stöckli, NASA Earth Observatory (NASA Goddard Space Flight Center).

2013; *Parker et al.*, 2011; *Oshchepkov et al.*, 2013; *Deng et al.*, 2014; *Frankenberg et al.*, 2013; *Boesch et al.*, 2013], and in the evaluation of carbon cycle models [*Basu et al.*, 2011; *Houweling et al.*, 2010; *Keppel-Aleks et al.*, 2013; *Mu et al.*, 2011; *Messerschmidt et al.*, 2013; *Fraser et al.*, 2013]. The TCCON instrumentation and previous versions of the software are described in detail in *Washenfelder et al.* [2006] and *Wunch et al.* [2011b]. The network consists of ground-based Fourier transform spectrometers that measure absorption of the direct solar beam in the near infrared region of the spectrum. The TCCON is over a decade old: its first dedicated instrument, located at Park Falls, WI, USA, was installed in May, 2004. The TCCON has since expanded to 23 operational sites; the site locations are plotted in Figure 1, and the site list with latitude, longitude, and altitude information is in Table 1. Information about sites that were previously part of the network is given in Table 2.

This paper describes the updates and improvements to the TCCON data for the GGG2014 data release, hosted at the Carbon Dioxide Information Analysis Center (CDIAC, `http://tccon.ornl.gov`). Previous versions of the TCCON data (GGG2009 and GGG2012) are also archived at CDIAC. Each TCCON dataset has an unique digital object identifier (DOI) that can be used to cite the data in scientific articles. The dataset citations are listed in Tables 1 and 2.

The TCCON data processing software, called "GGG", is centrally maintained at the California Institute of Technology. Each TCCON site uses the same version of the software, and the processing procedure is

consistent from site to site. The first step is to process the raw data (interferograms) into spectra, using a subroutine called "I2S" (interferogram-to-spectrum). *A priori* profiles of pressure, temperature, geopotential height, and water vapour from the National Centers for Environmental Protection and National Center for Atmospheric Research (NCEP/NCAR) reanalysis [*Kalnay et al.*, 1996] are generated for the days on which spectra are acquired. A subroutine called "GSETUP" generates empirical models of other trace gas profiles using the pressure and temperature profiles from the NCEP/NCAR reanalysis. The spectra are then passed into the main nonlinear least squares spectral fitting subroutine "GFIT" that iteratively scales the *a priori* atmospheric amounts to generate forward-modeled spectra that best fit the data. The retrieved total column amounts of the gases are in units of molecules cm^{-2} and tend to be strongly influenced by surface pressure (and hence topography). The total column amount, or VC_{gas}, is defined as the integral of the mole fraction of the gas ($f_{gas}(z)$), multiplied by the total number density ($n(z)$), from the surface altitude (z_s) to the top of the atmosphere:

$$VC_{gas} = \int_{z_s}^{\infty} f_{gas}(z) \cdot n(z) \cdot dz \tag{1}$$

Column-averaged dry-air mole fractions (DMFs; denoted $\mathrm{X_{gas}}$) are less sensitive to variations in surface pressure and atmospheric water vapour than the retrieved total column amounts. This characteristic is advantageous for carbon cycle studies because it permits direct comparisons of the trace-gas measurements during different seasons, between sites, and with *in situ* measurements. To calculate DMFs, the total column amount of the gas of interest is divided by the total column amount of dry air, which we measure using co-retrieved oxygen ($\mathrm{O_2}$) multiplied by an assumed dry-air mole fraction of $\mathrm{O_2}$ (0.2095).

$$X_{gas} = \frac{VC_{gas}}{VC_{O_2}} \times 0.2095 \tag{2}$$

By ratioing the column amounts, systematic errors that are common to *gas* and $\mathrm{O_2}$ cancel. The column-averaged amount of dry air ($\mathrm{X_{air}}$) is a special case, and a useful quantity we use to examine station-to-station biases, as it depends only on the surface pressure measurement (P_s), oxygen measurement (VC_{O_2}), and water column ($\mathrm{X_{H_2O}}$). The $\mathrm{X_{air}}$ value should therefore be identical at all sites. It is defined as:

$$\begin{aligned} X_{air} &= \frac{VC_{air}}{VC_{O_2}} \times 0.2095 - X_{H_2O} \times \frac{m_{H_2O}}{m_{air}^{dry}} \\ VC_{air} &= \frac{P_s}{\{g\}_{air} \cdot m_{air}^{dry}/N_a} \end{aligned} \tag{3}$$

The parameters m_{H_2O} (18.02 g mol^{-1}) and m_{air}^{dry} (28.964 g mol^{-1}) are the mean molecular masses of water and dry air, respectively, N_a is Avogadro's constant (6.022×10^{23} molecules mol^{-1}), and $\{g\}_{air}$ is the column-averaged gravitational acceleration. $\mathrm{X_{air}}$ is explicitly corrected for the influence of water (second term on the right hand side of equation 3). This correction is required because the surface pressure is enhanced by

the atmospheric water content. For an O_2 measurement with accurate spectroscopy, surface pressure, and H_2O retrievals, X_{air} would have a value of 1.0. However, the typical X_{air} value for TCCON measurements is ~0.98 and exhibits a small diurnal variation because of a ~2% bias in the O_2 spectroscopy that is airmass dependent. Large (~1%) deviations from 0.98 at any site indicate serious problems such as an error in surface pressure, spectra with ghosts, spectra with a poor instrument optical alignment, or an error in the time assigned to the spectrum causing the software to calculate the incorrect atmospheric path.

The dry-air mole fractions are passed through a set of post-processing routines, which include an airmass dependence correction, and a bias correction which ties the TCCON data to the currently-accepted World Meteorological Organization (WMO) scale through comparisons with WMO-calibrated *in situ* profile measurements obtained from aircraft or balloons.

There have been several important updates to the TCCON data processing software since the GGG2012 data version was released. These are: an interferogram resampling algorithm to correct for laser sampling errors (§2); improvements in the spectroscopy for CO, CH_4 and its isotopologues, H_2O, and N_2O (§3); improvements in the CH_4, HF, and N_2O *a priori* profiles (§4); and the ability to fit curvature in a spectrum's continuum (§5). As with all new versions of the TCCON data, an updated airmass dependence correction is calculated (§6) and the data are tied to the WMO through comparisons with co-located profiles measured by WMO-traceable instrumentation flown on aircraft and balloon platforms (§7). A GGG2014 error budget is presented in §8.

2 Laser Sampling Error Correction

The interferogram-to-spectrum (I2S) subroutine of GGG reads the raw data (the "interferogram"), applies a source intensity brightness correction [*Keppel-Aleks et al.*, 2007], a laser sampling error correction (new in GGG2014), a phase correction [*Mertz*, 1967], and a fast Fourier transform [*Bergland*, 1969] to compute the spectrum. The cause of the laser sampling error and its new correction method are described in this section.

The main instrument at each TCCON site is a Bruker 125HR Fourier transform spectrometer (FTS). There is a small subset of TCCON sites with an earlier model (the 120HR). Most of the sites possessing a 120HR FTS have upgraded electronics to 125HR-equivalents, and all the subsequent discussion is relevant to those sites. Sites with the 120HR without the upgrade include Lauder prior to 2011 (referred to as lauder01), Tsukuba prior to 2011 (tsukuba01), and Ny-Ålesund prior to 2012.

In all TCCON FTS instruments, a HeNe metrology laser with wavelength 632.8 nm (15798 cm^{-1}) is passed through the interferometer simultaneously with the solar (IR) beam and produces a sine wave output, which is used to sample the IR signal at precise and evenly spaced optical path differences (OPD). The resulting digitized IR signal is the interferogram. At most TCCON stations, data are recorded simultaneously

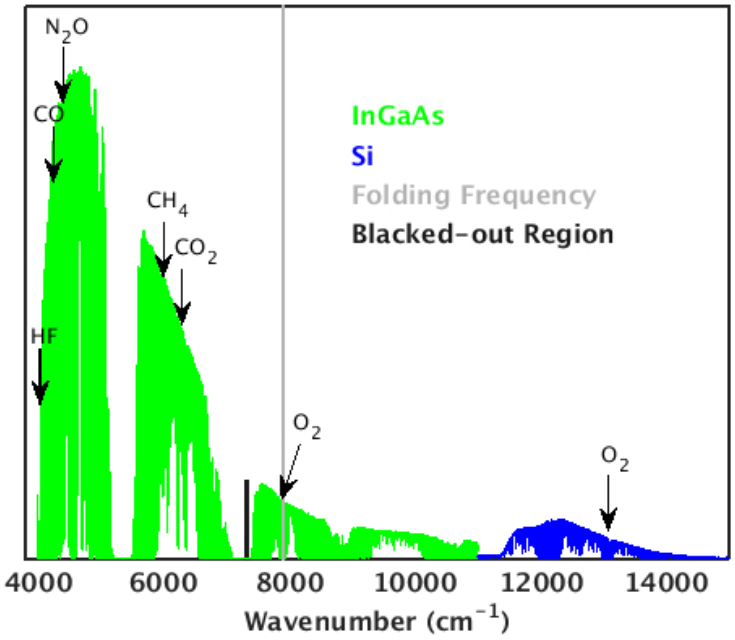

Figure 2: The spectral range covered by most TCCON stations. The InGaAs detector (green) covers 3800 cm^{-1}–11000 cm^{-1}, and the Si detector (blue) covers 11000 cm^{-1}–15000 cm^{-1}. The folding frequency at 7899 cm^{-1} is marked by the grey vertical line. Note that the InGaAs spectral region spans above and below the folding frequency (half the laser wavelength), requiring that the metrology laser is sampled twice per laser fringe. The Si spectral region is entirely above the folding frequency. Absorption features of the main gases of interest are marked by arrows. The O_2 band used in equation 2 is the band in the InGaAs region. H_2O and HDO are not shown because they absorb in many regions of the spectrum. The blacked-out region of the spectrum used in the *Dohe et al.* [2013] laser sampling error correction is marked in black (7290–7360 cm^{-1}).

on two detectors: an InGaAs detector, which is optically sensitive from 3800 cm^{-1} to 11000 cm^{-1}, and a Si detector, spanning 11000 cm^{-1} to 15000 cm^{-1} (Figure 2). All TCCON sites make measurements with an InGaAs detector, but not all are equipped with a Si detector. Because the InGaAs detector's spectral range spans both halves of the Nyquist range (i.e., the detector measures both above and below half the metrology laser wavenumber, 7899 cm^{-1}), the metrology laser must be sampled twice per laser cycle to uniquely resolve all frequencies. This is done by sampling the IR signal on both the rising and falling zero-crossings of the DC-coupled laser signal.

Messerschmidt et al. [2010] found that a faulty electronics board in Bruker 125HR Fourier transform spectrometers caused an error in the sampling of the metrology laser. In a correctly-sampled interferometer, samples on rising and falling zero-crossings of the DC-coupled laser signal are evenly spaced in OPD. In the faulty boards, however, the zero level was incorrect (it was not halfway between the peak and trough of the laser signal), and so the spacing of the samples was not even in optical path difference. This causes a small fraction of the spectral information above the Nyquist frequency (7899 cm^{-1}) to be folded back onto the

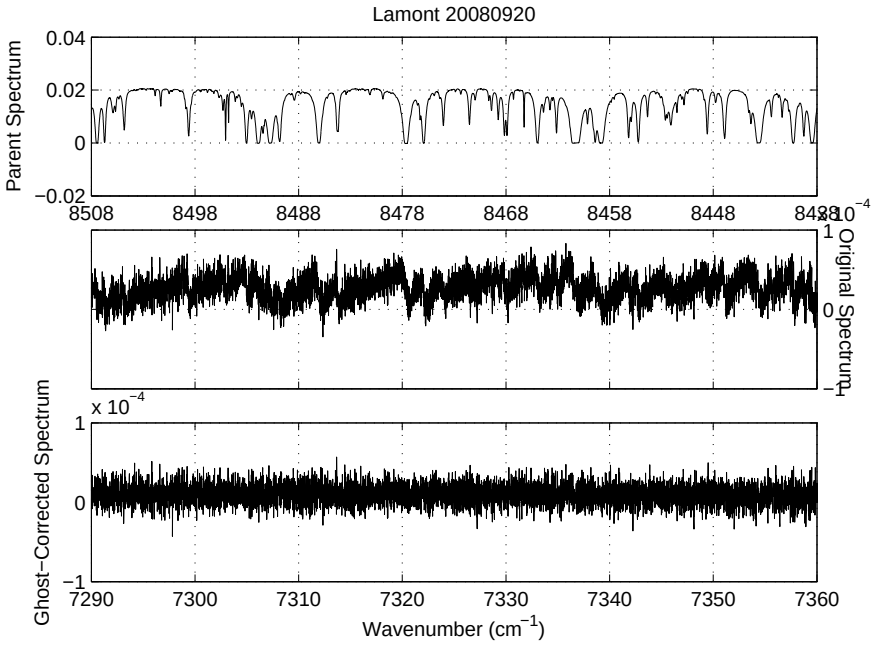

Figure 3: The top panel shows the parent region with reversed x-axis. The middle panel shows its ghost in the blacked-out region of the spectrum (7290–7360 cm^{-1}). The bottom panel shows the same blacked-out region of the spectrum after the I2S correction has been applied. These plots were created using averaged Lamont spectra on 2008/09/20, before the new laser sampling board was installed.

spectrum below 7899 cm^{-1}, and vice versa. This creates spurious signal called "ghosts" [*Brault*, 1996] that interfere with the spectral fitting. The retrievals of O_2 are most impacted by ghosts, as its absorption band straddles the 7899 cm^{-1} folding frequency (Figure 2). The magnitude of the ghosts relative to the desired ("parent") spectrum is proportional to the magnitude of the laser sampling error. Figure 3 shows a parent region (8438–8508 cm^{-1}) that creates visible ghosts in a typically blacked-out region of the main spectrum (7290–7360 cm^{-1}).

These ghosts can causes biases in X_{CO_2} of more than 1 ppm, but most TCCON instruments suffered from biases that were smaller. These errors, however, are site-dependent and can be time-dependent, as metrology lasers age and are replaced. As a consequence of the work of *Messerschmidt et al.* [2010], Bruker provided all TCCON partners with replacement laser sampling electronics boards to minimize this problem. Most TCCON sites installed the new boards in 2011, and since that time the laser sampling errors have been negligible. However, data recorded prior to the board replacement require correction.

There are two methods of correcting the TCCON spectra, the first of which is already described by *Dohe et al.* [2013]. This method uses spectra throughout the TCCON site's time series that are sufficiently wet (or of high enough airmass) to fully absorb a particular region of the spectrum (typically between 7290–7360 cm^{-1}, see Figure 2). The interferograms corresponding to the "wet" spectra are averaged over short

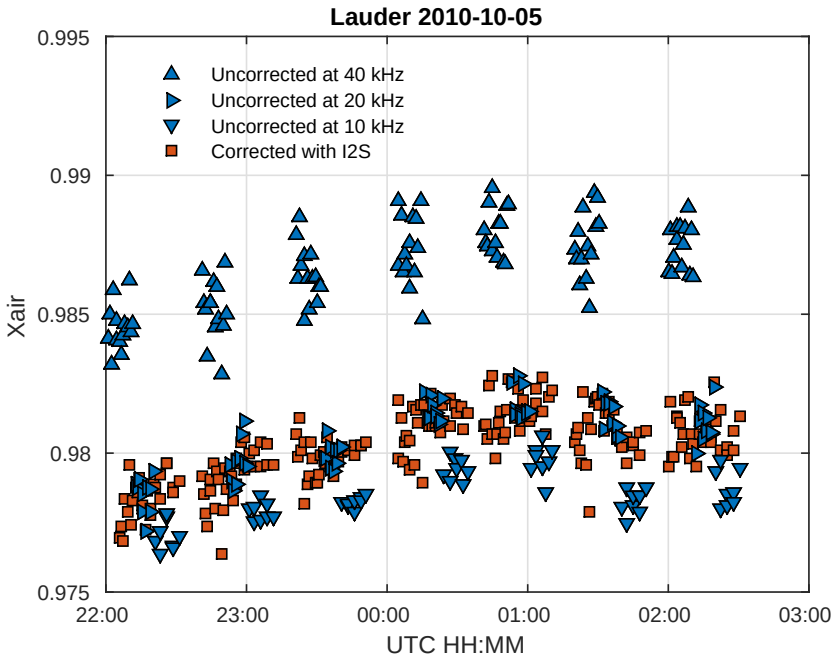

Figure 4: Retrieved X_{air} values during a day at Lauder where measurements were recorded while deliberately alternating the magnitude of the ghost (triangles) by modifying the scanning speed of the instrument. There are three sets of measurements: the 40 kHz set had the largest laser sampling error, the 10 kHz set had a smaller but non-zero laser sampling error, and the 20 kHz set had minimal laser sampling errors. The I2S method of correcting for the ghosts (squares) show good agreement with the measurements with minimal laser sampling errors.

time periods and passed through an algorithm that minimizes any spurious signal in the blacked out region by iteratively adjusting the resampled spectral spacing. The amount by which the interferogram must be resampled to minimize the spurious signal is then recorded and applied to all spectra. This method is intuitive and successful at minimizing ghosts, but is sensitive to detector non-linearities, requires *a priori* knowledge of the atmospheric H_2O amount, and cannot be performed on individual spectra due to insufficient signal-to-noise.

The second method of correcting the TCCON spectra makes use of the simultaneously-measured Si detector and will be referred to here as the "I2S" correction method. Because the Si detector spectral range is wholely contained in the upper half of the alias, but still sampled twice per laser wavelength, even and odd points in the interferogram each fully describe the resulting Si spectrum. Therefore, calculating the angle between the phase curves of the even-only and odd-only points of the Si interferogram provides a direct measure of the laser sampling error. This method does not require any *a priori* knowledge of the spectrum itself (i.e., whether it has blacked out regions), can be performed without iteration on every Si spectrum irrespective of the H_2O amount, and is insensitive to detector non-linearities. Because the

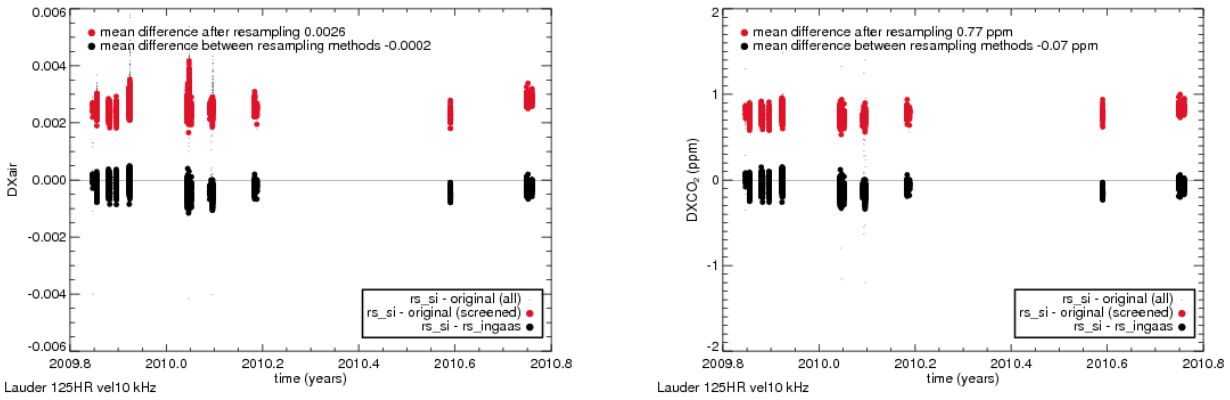

(a) X_{air} (b) X_{CO_2}

Figure 5: Retrieved values at Lauder from measurements recorded at 10 kHz, which had small but non-zero laser sampling errors. The red circles show the mean biases caused by the ghosts. The black circles show the mean differences between the I2S and *Dohe et al.* correction methods, which are an order of magnitude smaller than the biases caused by the ghosts. Shown in (a), the ghosts cause a bias in X_{air} of 0.0026; the difference between the I2S and *Dohe et al.* methods is -0.0002. In (b), for X_{CO_2}: 0.77 ppm, and -0.07 ppm.

Si and InGaAs spectra are recorded simultaneously and are digitized using the same laser signal, we can apply the laser sampling error calculated from the Si data directly to the InGaAs data. Figure 3 shows the results of the I2S method on the spectrum itself, and Figure 4 shows X_{air} retrievals from the Lauder 125HR (lauder02) instrument. The original Lauder X_{air} measurements cycled through three different values of the laser sampling error, induced by changing the scanning speed of the FTS. The X_{air} values, which should vary only slowly throughout the day, have marked discontinuities when the scan speed is changed. After applying the I2S correction, the retrieved X_{air} differences are negligible when the scan speed changes.

The main limitation of the I2S method is that the interferogram measured simultaneously with the InGaAs interferogram must be sufficiently over-sampled that the spectral signal occupies less than half the alias. At most TCCON stations, a Si diode detector is measured simultaneously with InGaAs and provides this over-sampled measurement. Karlsruhe is the exception, which simultaneously measures InGaAs and InSb, where the InSb range is limited by an optical filter to wavenumbers less than 7899 cm^{-1}. Over 90% of the TCCON data recorded have been corrected by the I2S method in the GGG2014 data version. Sites that do not possess the InGaAs/Si detector pair are: Eureka (eureka01), Ny Ålesund (nyalesund01), Bremen (bremen01), early Tsukuba (tsukuba01), early Lauder (lauder01), and Izaña (izana01).The Eureka instrument was installed with the new electronics board and does not suffer from ghosts. The tsukuba01, lauder01 and early Ny Ålesund 120HR instruments have different electronics to the Bruker 125HR, and likely do not suffer from ghosts. Bremen and Izaña use the *Dohe et al.* method to correct their ghosts. Figures 5(a)–(e) compare the *Dohe et al.* and I2S methods of correcting the laser sampling errors: the differences

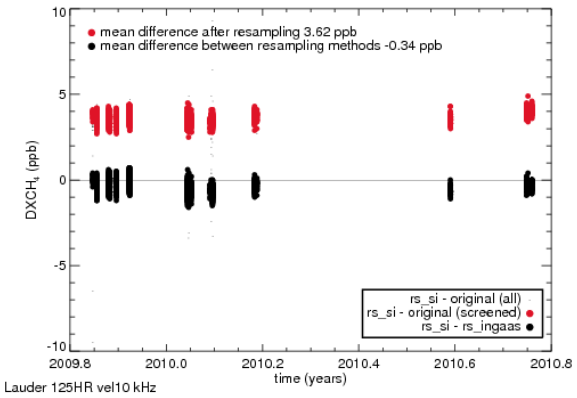

(c) X_{CH_4}

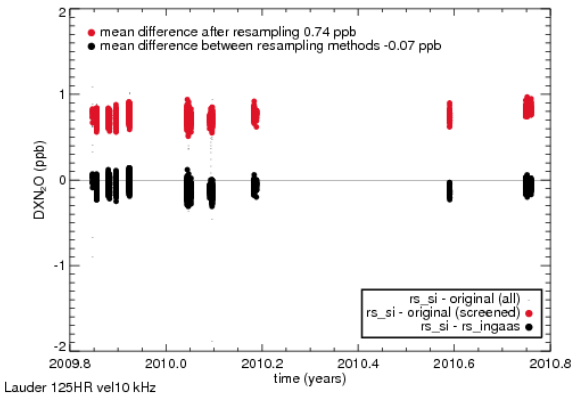

(d) X_{N_2O}

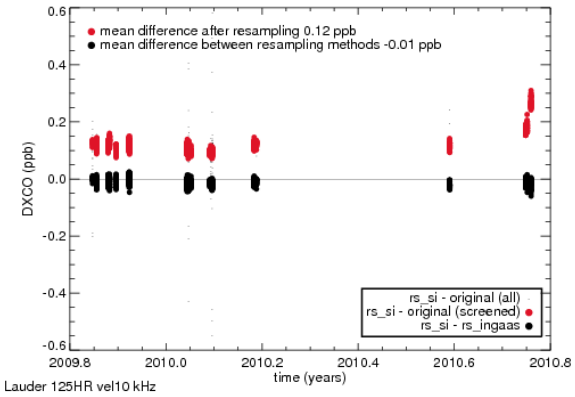

(e) X_{CO}

Figure 5: continued. In (c), for X_{CH_4}: 3.62 ppb, and -0.34 ppb. In (d), for X_{N_2O}: 0.74 ppb, and -0.07 ppb. In (e), for X_{CO}: 0.12 ppb, and -0.01 ppb.

between the two methods are negligibly small and an order of magnitude smaller than the errors induced by the uncorrected ghosts.

3 Updated Spectroscopy

GGG uses several types of spectroscopic line lists: atmospheric (telluric), solar, collision-induced absorption, self-induced absorption, and pseudo line lists. This section will discuss the updates to the atmospheric line list and the solar line list, which are most relevant to TCCON. The atmospheric line list [atm.101, *Toon*, 2014a] is available from `http://dx.doi.org/10.14291/tccon.ggg2014.atm.R0/1221656`. The solar line list [solar_merged.108, *Toon*, 2014b] is available from `http://dx.doi.org/10.14291/tccon.ggg2014.solar.R0/1221658`.

3.1 Atmospheric Line List

The main updates to the atmospheric line list for the GGG2014 software release are in the H_2O, CO, and $^{13}CH_4$ spectroscopy. An additional (10th) CO_2 isotopologue was added from the latest HITRAN database [HITRAN2012, *Rothman et al.*, 2013]. There were no other changes made to the CO_2 and O_2 spectroscopy. The windows fitted in GGG2014 are listed in Table 3. Below is an itemized list of changes to the spectroscopic line list.

- H_2O: There were many changes made throughout the $4000 - 6000$ cm^{-1} region based on fits made to Kitt Peak laboratory spectra. These changes not only affect the retrievals of H_2O and HDO, but also CO, N_2O, CH_4, and HF due to the water absorption in their windows.
- CH_4: A line list corresponding to $^{13}CH_4$ from HITRAN2012 (and tweaks) was added, which impacts the CO and CH_4 windows. There were several $^{13}CH_4$ lines in the previous line list that were mis-identified as $^{12}CH_4$ in the GGG2012 line list, and the mis-identified lines were removed.
- CO: We have adopted the HITRAN2012 line list, which has narrower widths than the HITRAN2008 line list used in GGG2012. After the combined changes from H_2O, $^{13}CH_4$, and CO, the two CO windows produce more consistent retrieval results. For GGG2012, there was a 3-5% difference in the retrieved CO columns between windows. For GGG2014, the difference has reduced by about an order of magnitude, to 0.1-0.6%.
- N_2O: In addition to the improved H_2O line list in the region, we have added an additional retrieval window (centred at 4719 cm^{-1}) to improve the robustness of the N_2O retrievals.

3.2 Solar Line List

Absorption and emission lines from the sun itself are modeled in GGG using a solar line list that contains more than 40,000 lines covering $600 - 25,000$ cm^{-1}. Combined with a simple empirical line shape model, the line list can be used to generate a solar pseudo-transmittance spectrum at any spectral grid, for disk-center, disk-integrated, and intermediate cases. The line list was calculated from high-resolution spectra from Kitt Peak [*Wallace and Livingston*, 2003], MkIV balloon [*Toon*, 1991], TCCON, and ATMOS [*Irion et al.*, 2002], and was subsequently validated by ACE-FTS [*Bernath*, 2005], TCCON, GOSAT [*Hamazaki*, 2005; *Kuze et al.*, 2009], Kitt Peak [*Kurucz*, 2005, 2008], and SolSpec [*Thuillier et al.*, 2003] measurements. The GGG2014 solar line list is very similar to the GGG2012 solar line list in the TCCON frequency range.

4 Improved *a priori* profiles

A priori profiles in GGG are generated by a set of empirical functions that are optimized to fit *in situ* measurements from balloon-borne platforms (MkIV [*Toon*, 1991], AirCore [*Karion et al.*, 2010], OMS [*Daube Jr. et al.*, 2002]), aircraft (HIPPO [*Wofsy*, 2011], START-08 [*Pan et al.*, 2010], INTEX-NA [*Singh et al.*, 2006], IMECC [*Messerschmidt et al.*, 2011; *Geibel et al.*, 2012]), and satellites (ACE-FTS [*Bernath*, 2005], ATMOS [*Irion et al.*, 2002]). The empirical functions include a secular increase, interhemispheric gradient, seasonal cycle, and stratospheric decay based on the age of air. The GGG2014 *a priori* profiles can be generated using a stand-alone Fortran program [*Toon and Wunch*, 2014], available from `http://dx.doi.org/10.14291/tccon.ggg2014.priors.R0/1221661`.

There have been small improvements to the GGG2012 *a priori* profiles to produce the GGG2014 profiles. The main change is in the calculation of the tropopause altitude, which is now computed internally from the NCEP temperature profile. In GGG2012, we relied on NCEP's calculation of tropopause pressure, provided separately from the temperature profile. The change to internally-calculated tropopause altitudes resulted in differences of less than 1 km. Figure 6(a) shows the GGG2012 and GGG2014 *a priori* profiles and their differences at Lamont, and Figure 6(b) shows the *a priori* profiles and differences for Lauder. The main differences for each gas are:

- CH_4: The secular increase was modified from 0.4%/yr to 0.3%/yr.
- CO: The interhemispheric gradient was increased by $\sim$ 10%, making it more realistic. The secular decrease was modified from -0.5% to -0.6%/year.
- N_2O: No significant changes, except for the tropopause altitude calculation.
- HF: A secular decrease of 1% per year was added. There was previously no secular dependence in the HF *a priori*.
- CO_2: The secular increase was slightly modified from 0.54%/yr to 0.52%/yr.
- H_2O and HDO: The manner in which specific humidity from NCEP is converted to mixing ratio was changed to avoid values$>$ 1, causing up to one percent difference in the lowest altitudes under warm, humid conditions. Above 300 hPa, changes occurred due to the new calculation of the tropopause altitudes.

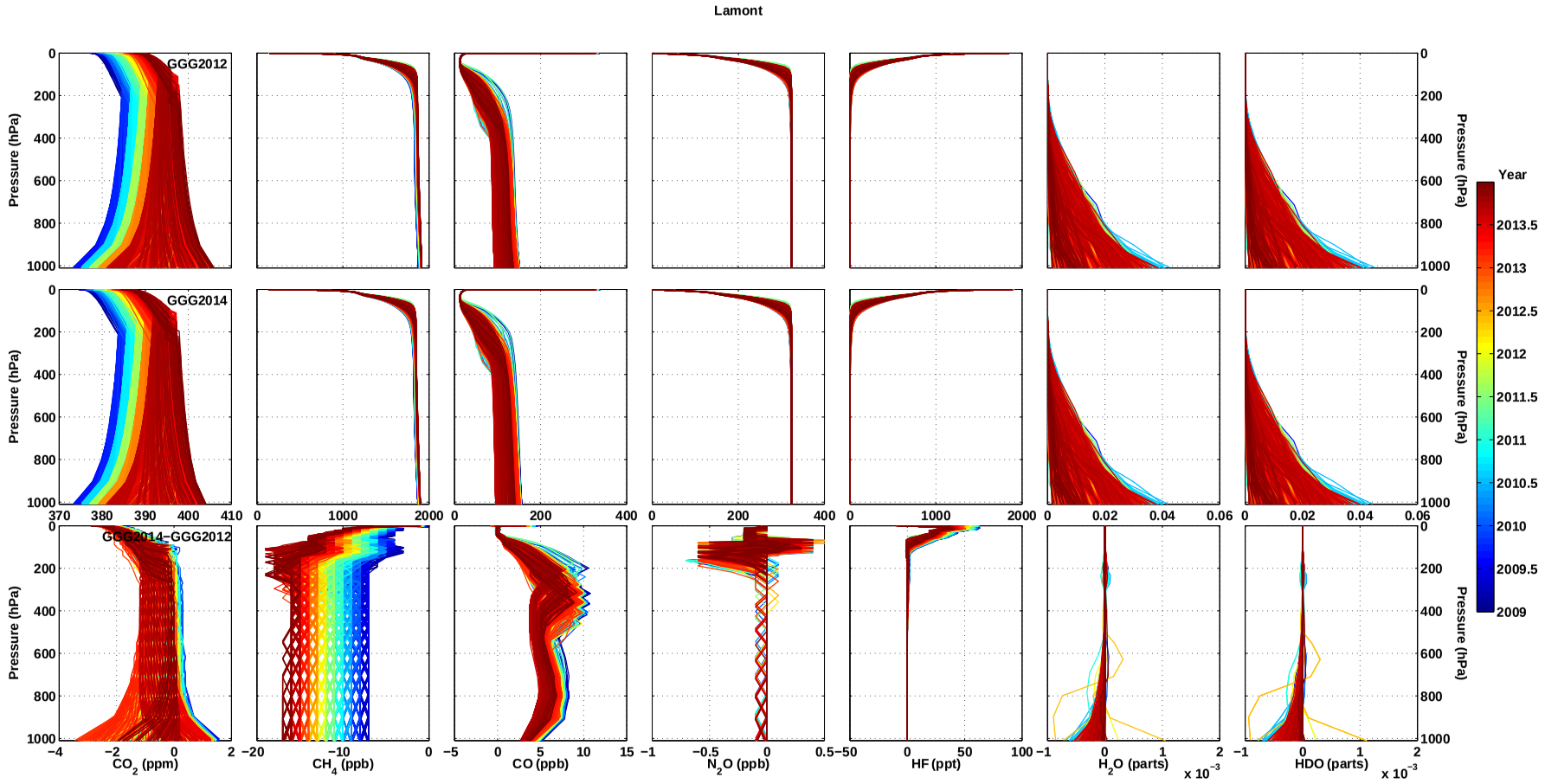

(a) Lamont

Figure 6: The differences in the Lamont (a), and Lauder (b) *a priori* profiles between GGG2012 and GGG2014. The top panels of each figure are the GGG2012 *a priori* profiles, the middle panels are the GGG2014 *a priori* profiles, and the bottom panels are the differences between them. The colours represent the time.

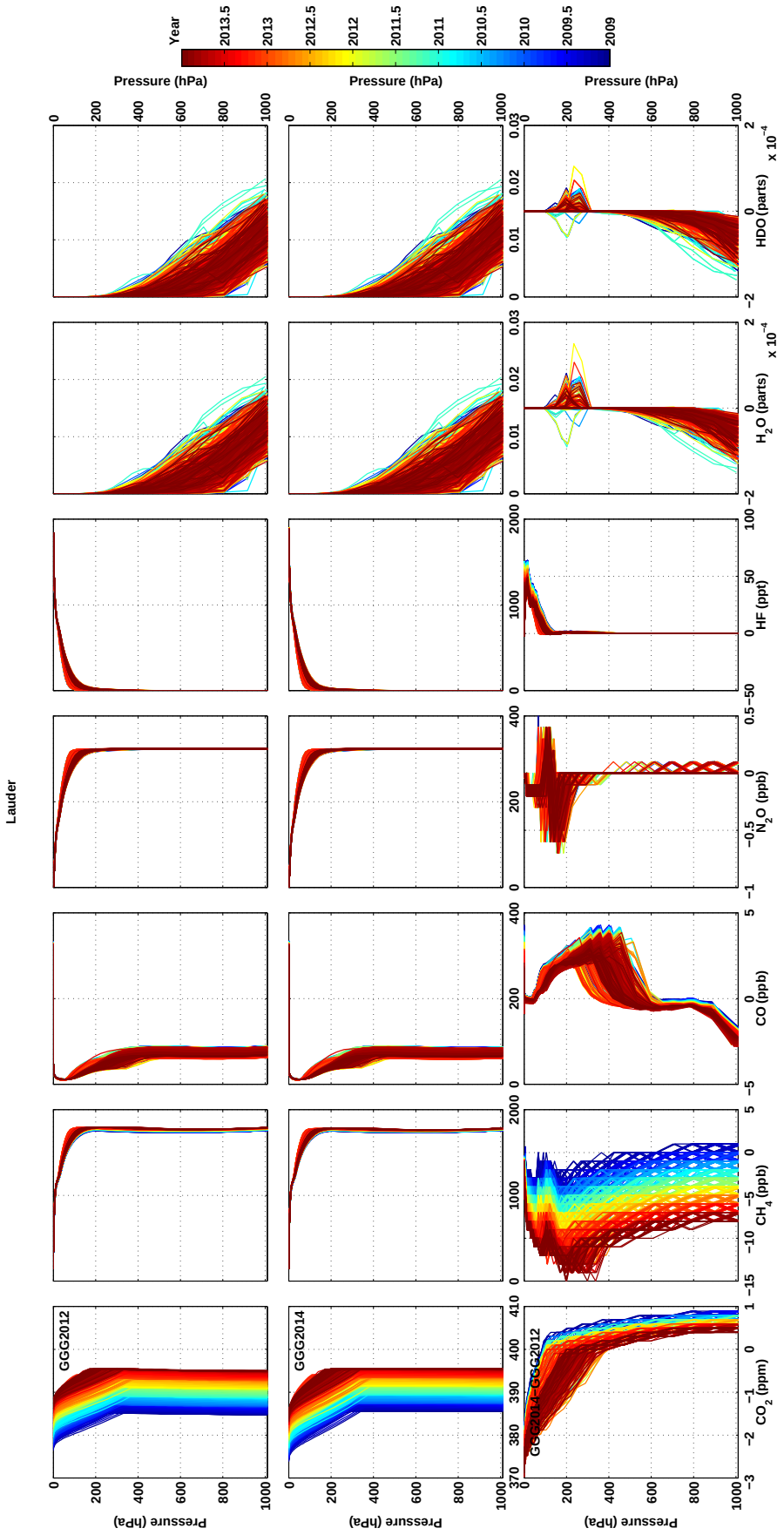

(b) Lauder

Figure 6: continued.

5 Continuum Curvature

TCCON spectra are not radiometrically calibrated, and thus the fitted spectra include the responses of the instrument and the solar Planck function, which GFIT attempts to fit. In all previous versions of GFIT, a level and tilt were fitted to the continuum of each spectrum. GGG2014 has the ability to fit higher order polynomials to the continuum level. This option allows the fitting of curvature in the continuum level of the spectrum that is caused by instrument features (e.g., an optical filter with a wavy bandpass, a beamsplitter transmission shape, etc.). The continuum curvature fitting option should not fit out spectroscopic errors, as they should be modeled separately.

This feature is not a standard fitted parameter in the TCCON data processing for GGG2014. The exception to this is for the Karlsruhe TCCON station that has an unique optical setup with significant higher-order continuum curvature that requires this feature to properly and robustly fit the spectra [*Kiel et al.*, in prep.]. The standard TCCON setup does not have the same significant curvature. However, as the widths of our fitting windows increase, and the spectroscopic line lists improve, small continuum curvature will become more important to the spectral fits. It is likely that continuum curvature will be a standard fitted parameter in subsequent versions of GGG.

6 Updated airmass dependence correction

For most gases, the dry-air mole fractions (DMF) measured at noon appear systematically larger than at sunrise or sunset by up to 1%. This has been shown to be an artifact resulting from spectroscopic inadequacies and instrumental problems. The formulation for calculating the airmass dependence is described in detail in *Wunch et al.* [2011b], but briefly, symmetric and antisymmetric components of X_{gas} about local noon are calculated for each day. The average symmetric component is considered to be spurious, and removed from the final X_{gas} amount.

To calculate new airmass dependent correction factors for GGG2014, we used the Park Falls, Lamont and Darwin time series, and compared their daily symmetric diurnal components. The median value of the three sites is applied network-wide, if the values at the three test sites are consistent. The results are listed in Table 4 and plotted in Figure 7. We would not expect a change in the airmass dependence calculated for X_{CO_2} since there have been no significant changes to the O_2 and CO_2 spectroscopy, and indeed this is the case. Similarly, the airmass dependence of X_{CH_4} was only slightly modified. Due to the improvements in the H_2O spectroscopy in the N_2O windows, the airmass dependence in X_{N_2O} reduced significantly from $+0.0172$ to $+0.0039$. The X_{CO} airmass dependence, which was inconsistent between the three test sites for GGG2012, is much more consistent for GGG2014, again, due to the significant improvements in the CO spectroscopy, and a value of -0.0483 has been adopted for GGG2014.

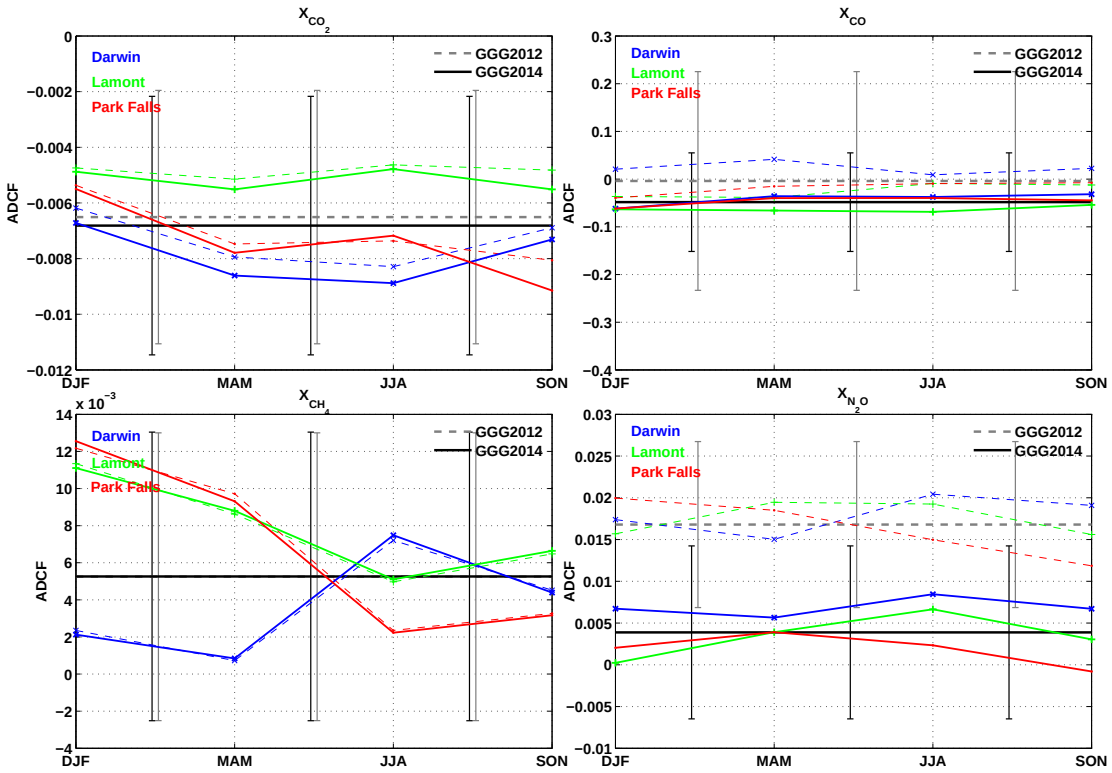

Figure 7: The unitless airmass dependent correction factors (ADCF) for Darwin (blue), Lamont (green) and Park Falls (red), as a function of season. The dashed lines are the values for GGG2012, and the solid lines are the values for GGG2014.

7 Updated aircraft bias correction

The absolute accuracy of the TCCON column amounts is limited by spectroscopic uncertainties to $2-3\%$, which is insufficiently accurate for carbon cycle studies. But since these spectroscopic biases tend to be highly reproducible, site to site, and day to day, they can in principle be removed from the data. To tie the TCCON measurements to the currently-accepted World Meteorological Organization (WMO) gas standard scale, precise and accurate *in situ* instrumentation are flown on airborne platforms over the TCCON stations, and measure profiles of the gases of interest while the ground-based TCCON station is measuring the total column amounts. The *in situ* profiles are then integrated, following the method described in *Wunch et al.* [2010], taking into account the TCCON *a priori* profiles and column averaging kernel. The integrated profiles are compared with the TCCON retrieval results, and a scaling factor is calculated and applied to the TCCON data. There are more than 30 independent profiles of CO_2 compared with TCCON measurements, which essentially removes the spatially invariant systematic biases (e.g., spectroscopy) from the DMFs.

For each version of the GGG spectroscopy, new scaling factors need to be calculated and applied to the TCCON data. Any additional profiles measured over the TCCON sites are also added to the comparisons

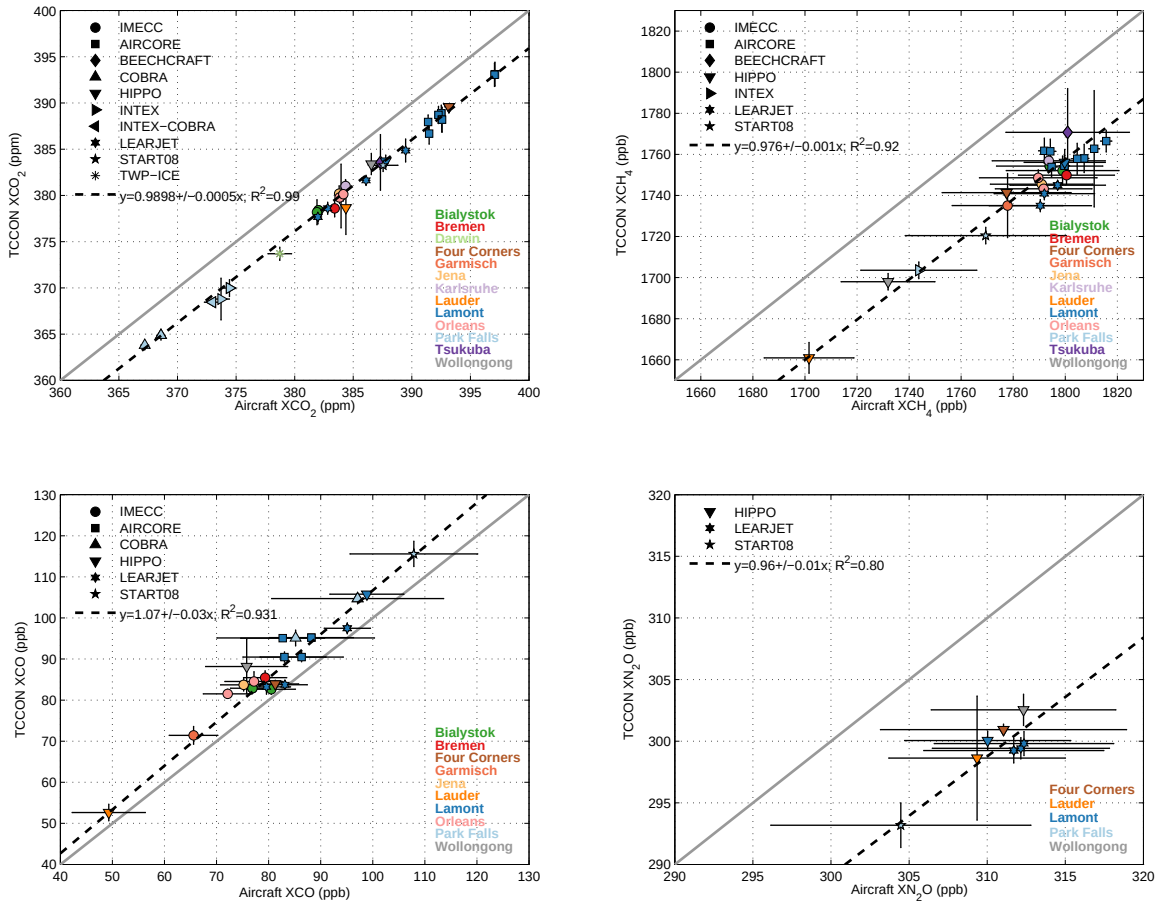

Figure 8: The X_{CO_2}, X_{CH_4}, X_{CO}, and X_{N_2O} calibration curves for GGG2014.

to ensure that the slopes are robust both over time and from site to site. For GGG2014, we added several AirCore profiles over Lamont, several IMECC profiles over the European TCCON stations [*Messerschmidt et al.*, 2011; *Geibel et al.*, 2012], and a HIPPO profile over Four Corners (see Tables 5–9 for a list of profiles). As a result of adding these additional profiles, it became necessary to add a digit to the slope between the TCCON and *in situ* measurements. The additional digit caused an overall difference between GGG2012 and GGG2014 X_{CO_2} of 0.3 ppm (with the GGG2014 results smaller).

The GGG2014 aircraft and AirCore comparison yielded small changes in the TCCON bias corrections for X_{CO_2} and X_{CH_4} (Table 4). The slopes are closer to 1 for X_{N_2O} and X_{H_2O}, and further from 1 for X_{CO}. The plots in Figure 8 illustrate the excellent agreement between the WMO-standard airborne measurements and the TCCON measurements.

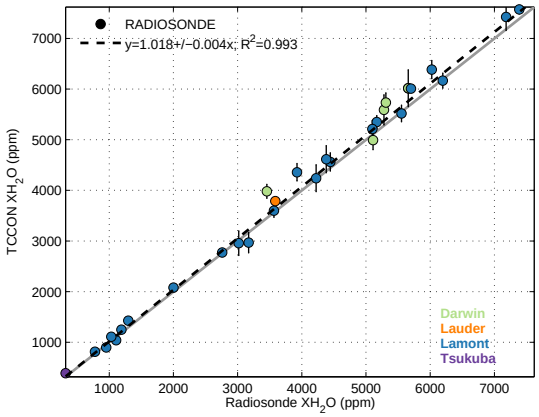

Figure 8: continued, showing the X_{H_2O} calibration curve for GGG2014.

8 Uncertainty Budget

This section presents a sensitivity study, following *Wunch et al.* [2011b], whereby each known source of uncertainty is perturbed by a realistic amount in the GFIT forward model, and the fractional difference in X_{gas} for each uncertainty source, relative to the unperturbed case, is computed. These sensitivities are computed for each retrieved X_{gas} from spectra recorded on three clear days in Lamont (2013-04-11, 2013-05-22, 2013-06-26), which span a large difference in atmospheric water vapour, and a large range of solar zenith angles (SZAs) and surface temperatures (Figure 9). The total uncertainty is the sum in quadrature of each individual uncertainty. The only uncertainty source previously included in the *Wunch et al.* [2011b] paper, but not included here is random error, which does not cause a bias. The sensitivites assessed are listed below.

- ***A priori* profiles** are modified for X_{CO_2}, X_{CH_4}, X_{N_2O}, X_{CO}, X_{HF}, and X_{air} by shifting the profiles down by 1 km. The profiles are modified for X_{H_2O} and X_{HDO} by reducing the value of the surface concentration by 50%.
- ***A priori* temperature profiles** are increased by 1K at all altitudes.
- ***A priori* pressure profiles** are increased by 1 hPa at all altitudes.
- **Zero level offsets** are increased by 0.1% to test the sensitivity of our retrievals to modest detector nonlinearity.
- **Pointing offsets** are increased by 0.05°, which is ∼20% of the solar radius. This causes an error in the estimated airmass for a given spectrum.
- **Continuum curvature** is modified by fitting a third order continuum curvature to all windows wider than 20 cm^{-1} (see Table 3), using the new continuum curvature option (§5).

- **Surface pressure** is modified by adding 1 hPa, the largest pressure error permitted by the TCCON data protocol.
- **Observer-sun Doppler stretch (osds)** is modified by adding 2 ppm. This causes the solar lines to be Doppler-shifted relative to the telluric lines, creating systematic residuals in the spectral fits.
- **Shear misalignment** is modified by creating an instrument line shape (ILS) with a significantly reduced modulation efficiency (ME) at zero path difference (ZPD) relative to maximum OPD. This results in a narrower line than the theoretical ILS that is assumed by the GGG forward model [*Wunch et al.*, 2011b, §A(c)(ii)]. We assume a Lorentzian form for the ME error as a function of OPD (x, equation 4), choosing α such that the ME is lower by 5% at ZPD than at maximum OPD, the largest shear misalignment permitted by the TCCON data protocol.

$$\mathrm{ME}(x) = \frac{\alpha}{1 + (0.5x)^2} \tag{4}$$

- **Angular misalignment** is modified by creating an ILS with a significantly lower ME at maximum OPD relative to ZPD, resulting in broader lines than the theoretical ILS predicts. The equation describing the ME error is a quadratic function of OPD (x) written in equation 5 below. Here, α was chosen to approximate a ME of 0.95 at maximum OPD, the largest angular misalignment permitted by the TCCON data protocol.

$$\mathrm{ME}(x) = 1 - (\alpha x)^2 \tag{5}$$

- **Field of view (fov)** is increased by 7% to reflect any uncertainty in the field stop diameter in the instrument.

The results for each day are shown in Figure 10, and the totals for each day are shown in Figure 11. The largest contributors to TCCON's uncertainty budget for all gases are shear misalignments, osds, *a priori* profile shape errors, *a priori* temperature profile errors, continuum curvature, and zero-level offsets. The results for each gas are discussed in turn below.

8.1 X_{CO_2}

The X_{CO_2} results are very similar to those in *Wunch et al.* [2011b]: the errors are below 0.25% (∼1ppm) until the solar zenith angles are larger than ∼82°. The largest sources of error are shear misalignments, continuum curvature, osds, and *a priori* temperature. At higher solar zenith angles, zero-level offsets become significant.

We also looked at the X_{CO_2} sensitivity to a larger variety of *a priori* profile shapes (Figure 12). We tried setting the *a priori* profile to a constant (400 ppm) through the entire vertical column, and to a constant (400 ppm) in the troposphere while matching the TCCON *a priori* profile in the stratosphere. We felt that

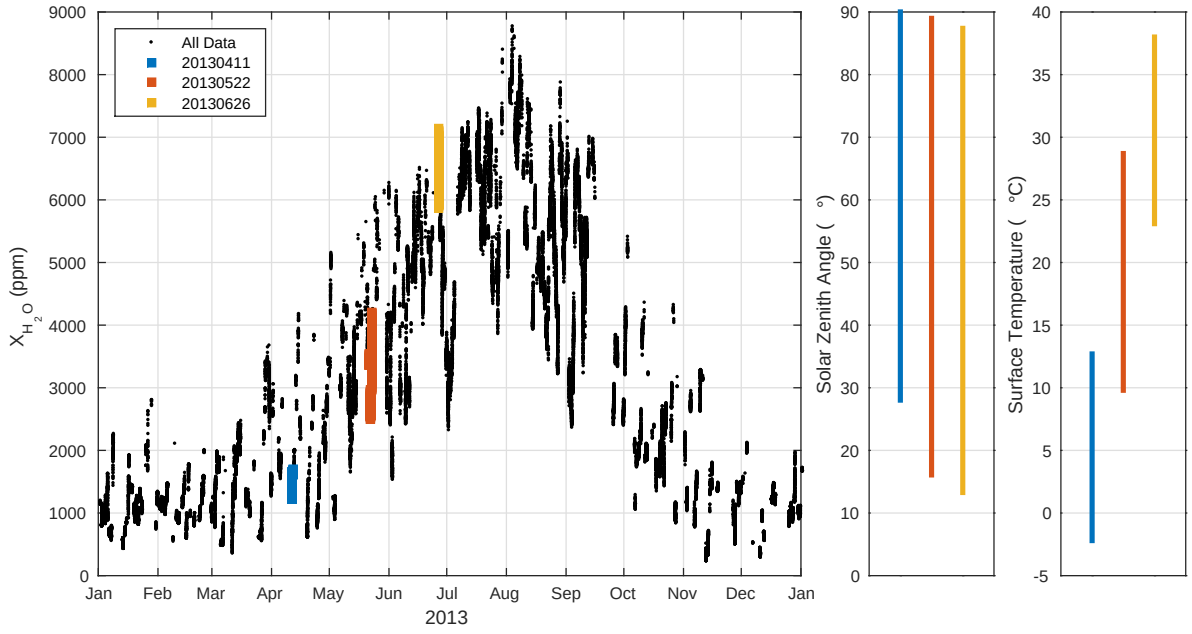

Figure 9: The water record at Lamont during 2013, showing the three dates chosen for the error budget analysis. The right two panels show the span in solar zenith angle and surface temperature for the three days.

these were too extreme to be included in a reasonable total error budget, but it is interesting to see how a grossly incorrect *a priori* profile shape will impact the retrieved X_{CO_2}. For the constant profile, the errors can reach 0.4% in the winter, when the tropopause height is lowest and the surface fluxes of CO_2 are strongly positive.

8.2 X_{CH_4}

The X_{CH_4} errors are below 0.5% (∼5ppb) until the solar zenith angles are above ∼85°. The largest sources of error are osds, shear misalignment, continuum curvature, *a priori* profile shape, and angular misalignment. At high solar zenith angles, the zero-level offsets and *a priori* temperature profile become signficant.

8.3 X_{N_2O}

The X_{N_2O} errors are ∼1% (∼3ppb) and reasonably independent of solar zenith angle. The largest sources of error are shear misalignment, *a priori* profile shape, osds, and zero level offsets. At high solar zenith angles, the *a priori* temperature profile and pointing offsets become signficant.

8.4 X_{CO}

The X_{CO} errors are below 4% and decrease with solar zenith angle. The largest source of error is the osds, which is unsurprising given that for every telluric CO line in the spectrum, there is also a solar CO line lurking beneath. The shear misalignment, continuum curvature, and *a priori* profile shape are the other leading sources of error.

The next version of GGG will independently fit the solar-gas stretch from the telluric lines in a window, and that will significantly reduce the retrieval's sensitivity to errors in the osds. Figure 13 illustrates this point.

8.5 X_{air}

The X_{air} errors are below 0.5% at solar zenith angles less than ∼78°. The largest source of error is the zero-level offsets, shear misalignment, and pointing offsets.

8.6 X_{H_2O}

The X_{H_2O} errors are at or below 1.3% below ∼85° solar zenith angle. The largest source of error is the *a priori* profile shape, followed by osds, and the *a priori* temperature profile.

8.7 X_{HDO}

The X_{HDO} errors are below 2% for all solar zenith angles. The largest source of error is the *a priori* profile shape, followed by osds, shear misalignment, and the *a priori* temperature profile. Contrary to the other gases, the X_{HDO} error is significantly different for the three dates, which differ in their total water column amounts, and atmospheric temperatures. This difference could be due to water interference, or it could be due to an inappropriate *a priori* profile shape.

8.8 X_{HF}

HF has only a single absorption line (4038.96 cm^{-1}) so the retrievals tend to be quite noisy, especially at high solar zenith angles. The X_{HF} errors are at or below 8% below ∼80° solar zenith angles. The largest sources of error are the *a priori* profile shape, the shear misalignment and angular misalignment. At higher solar zenith angles, and when the atmosphere is wetter, X_{HF} is a difficult molecule to measure in this spectral region, as its absorption line resides on the wing of a strong water line. For this reason, the total error cannot be computed for the wettest of the three days (2013-06-26).

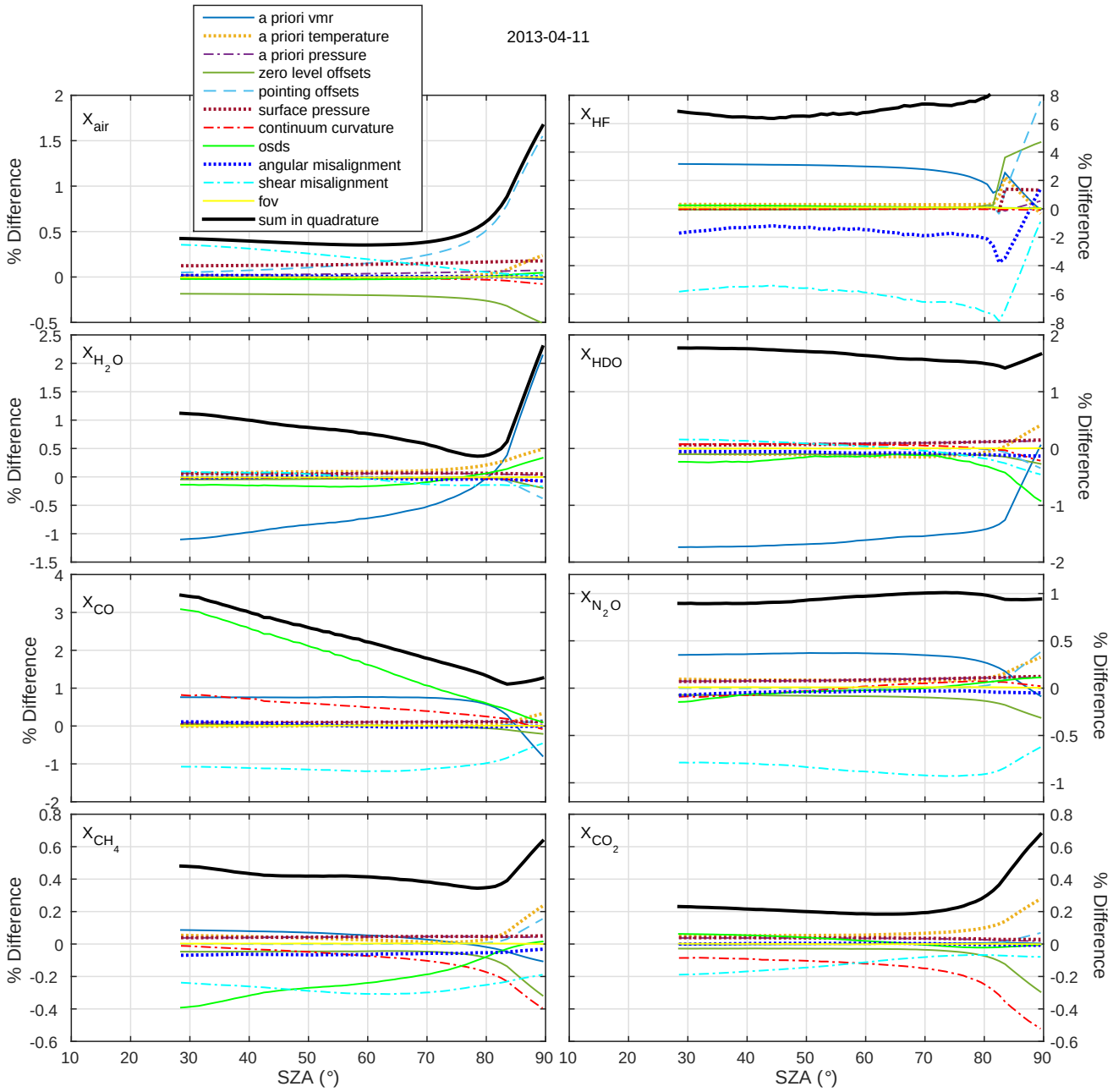

(a) 2013-04-11

Figure 10: The uncertainty budget for each known source of uncertainty for all retrieved gases for GGG2014 on 2013-04-11 (a), 2013-05-22 (b), and 2013-06-26 (c). The data plotted are the differences from the standard GGG product in percent.

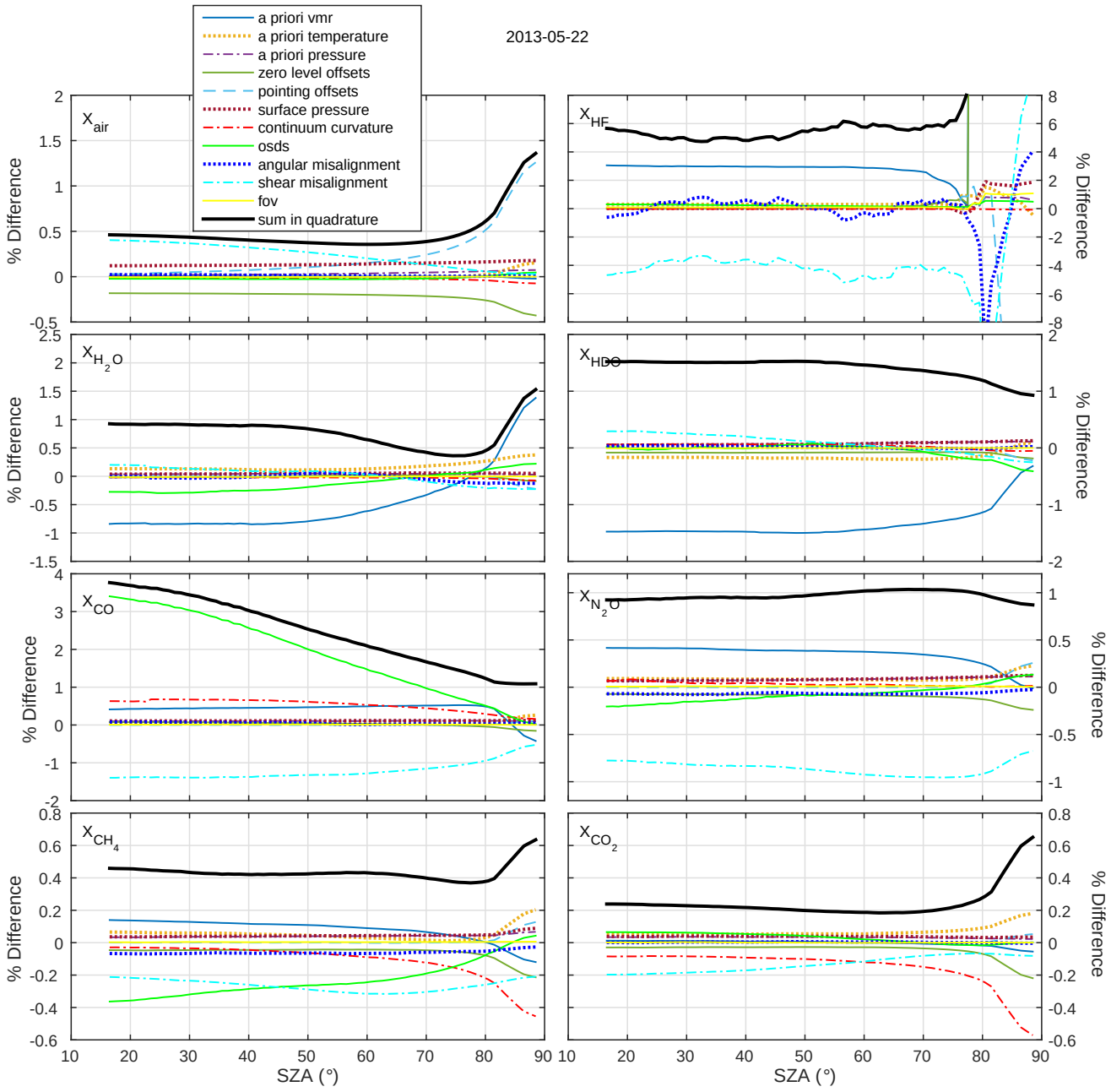

(b) 2013-05-22

Figure 10: continued.

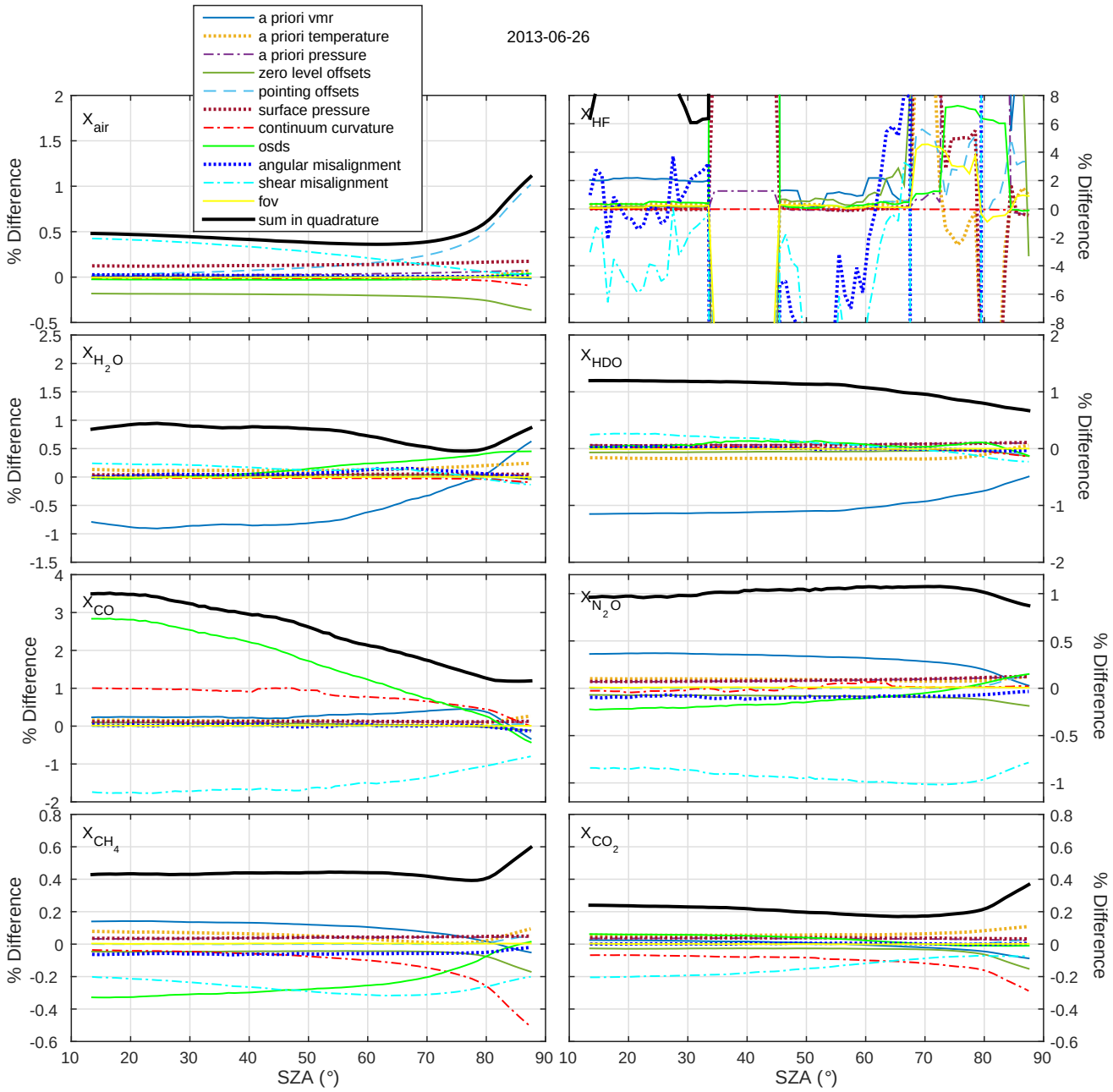

(c) 2013-06-26

Figure 10: continued.

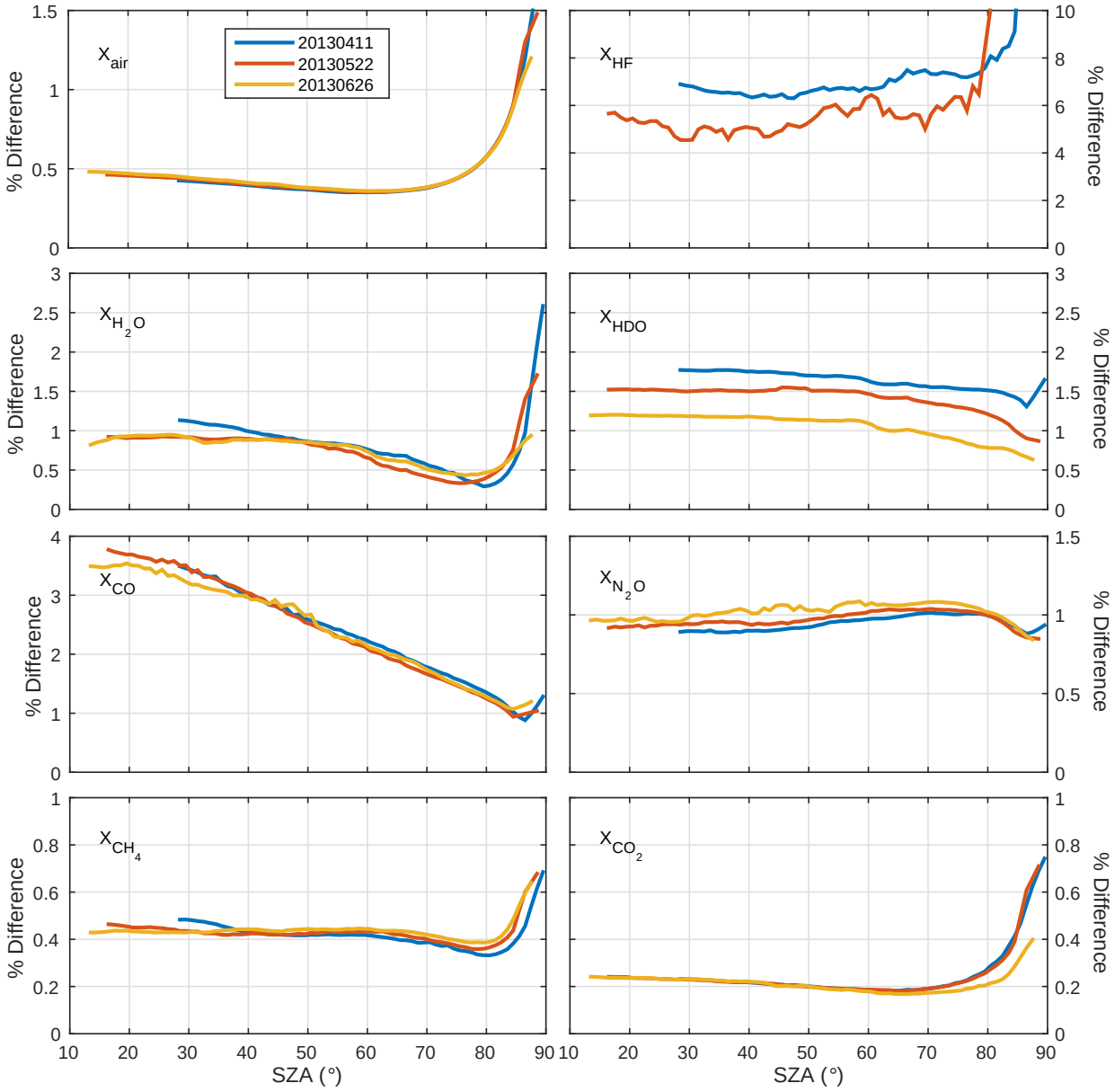

Figure 11: The total uncertainty budget for all retrieved gases for GGG2014. The 2013-06-26 uncertainty budget for X_{HF} is not shown here because the window was mostly blacked out due to a large line-of-sight water column.

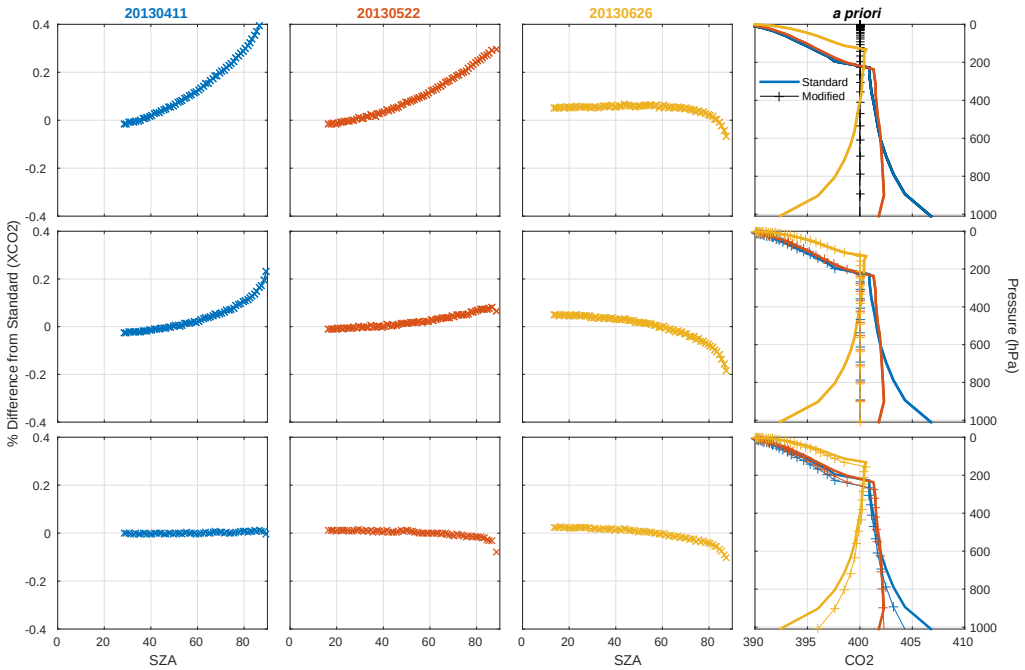

Figure 12: The effect of different CO_2 *a priori* profiles on the retrieved X_{CO_2} as a function of solar zenith angle. The top panel uses a single value of X_{CO_2} (400 ppm); the middle panel uses 400 ppm up to the tropopause, and the TCCON prior in the stratosphere; the bottom panel uses the TCCON prior shifted down by 1 km. The effect of the shifted TCCON prior is included in the total uncertainty budget.

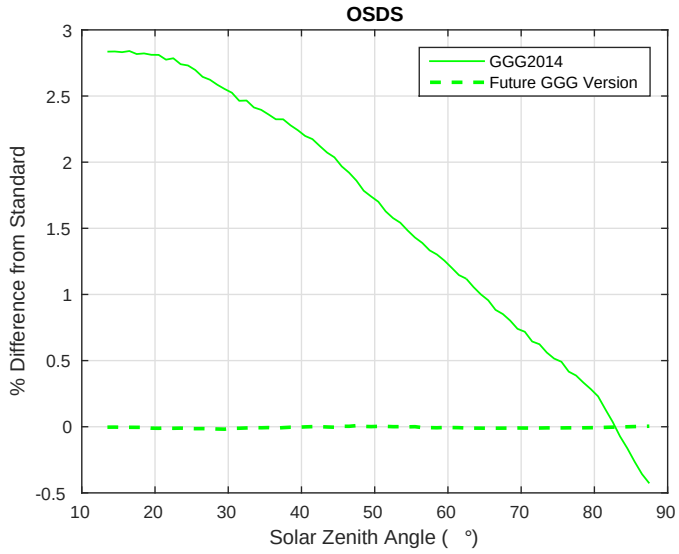

Figure 13: The difference in retrieved X_{CO} caused by an observer-sun Doppler stretch of 2 ppm without (solid) and with (dashed) a fitted solar-gas stretch for 2013-06-26 at Lamont. GGG2014 does not feature a fitted solar-gas stretch; future versions will include this feature, reducing the retrieval sensitivity to error in the OSDS.

9 Conclusions and Future Work

The GGG2014 version of the TCCON data represent a significant improvement in network-wide consistency over the GGG2012 data set. This is mainly due to a new algorithm that corrects for laser sampling errors (§2), and improved spectroscopy in H_2O, CO, and $^{13}CH_4$ (§3). The GGG2014 TCCON data are available to the public through the CDIAC archive system (`http://tccon.ornl.gov`).

The uncertainty budget in §8 indicated the leading-order error terms, which will guide our work for future GGG software versions. These leading-order terms and potential solutions are:

- Fitting solar-gas stretches instead of assuming that the solar tracker is pointing at the centre of the sun. This will greatly reduce the "osds" impact on the retrievals.
- Correcting the retrieved values for errors in the temperature profile. This will reduce the errors from the "*a priori* temperature".
- Using a real ILS instead of assuming a perfect ILS. This will reduce the errors from the "shear" and "angular" misalignment.
- Fitting all TCCON data with consistent orders of continuum curvature. This will reduce potential errors from improperly fitting the continuum levels of the spectra.
- Fitting the zero level offsets in the spectra.
- Continued improvements to the *a priori* profiles, and in particular, their shapes.

Acknowledgements

We thank CDIAC for their support and expertise in data archiving. We thank NIES for supporting TCCON through the GOSAT project. We thank the OCO-2 project for supporting the TCCON infrastructure and NASA for supporting TCCON under grant NNH13ZDA001N-CARBON. We thank our TCCON Partners for their scholarship, diligence, meticulousness, enthusiasm, and FTS expertise. Part of the work described in this paper was performed at the Jet Propulsion Laboratory, California Institute of Technology, under a contract with NASA.

References

Basu, S., et al. (2011), The seasonal cycle amplitude of total column CO 2 : Factors behind the model-observation mismatch, *Journal of Geophysical Research*, *116*(D23), 1–14, doi:10.1029/2011JD016124.

Bergland, G. (1969), A radix-eight fast Fourier transform subroutine for real-valued series, *IEEE Transactions on Audio and Electroacoustics*, *17*(2), 138–144, doi:10.1109/TAU.1969.1162043.

Bernath, P. F. (2005), Atmospheric Chemistry Experiment (ACE): Mission overview, *Geophysical Research Letters*, *32*(15), 1–5, doi:10.1029/2005GL022386.

Boesch, H., N. M. Deutscher, T. Warneke, K. Byckling, A. J. Cogan, D. W. T. Griffith, J. Notholt, R. J. Parker, and Z. Wang (2013), HDO/H2O ratio retrievals from GOSAT, *Atmospheric Measurement Techniques*, *6*(3), 599–612, doi:10.5194/amt-6-599-2013.

Brault, J. W. (1996), New approach to high-precision Fourier transform spectrometer design, *Applied Optics*, *35*(16), 2891–6.

Butz, A., et al. (2011), Toward accurate CO2 and CH4 observations from GOSAT, *Geophysical Research Letters*, *38*(14), 2–7, doi:10.1029/2011GL047888.

Chevallier, F., et al. (2011), Global CO 2 fluxes inferred from surface air-sample measurements and from TCCON retrievals of the CO 2 total column, *Geophysical Research Letters*, *38*(24), 1–5, doi:10.1029/2011GL049899.

Daube Jr., B. C., K. A. Boering, A. E. Andrews, and S. C. Wofsy (2002), A high-precision fast-response airborne CO2 analyzer for in situ sampling from the surface to the middle stratosphere, *Journal of Atmospheric and Oceanic Technology*, *19*(10), 1532–1543, doi:10.1175/1520-0426(2002)019⟨1532:AHPFRA⟩2.0.CO;2.

Deng, F., et al. (2014), Inferring regional sources and sinks of atmospheric CO2 from GOSAT XCO2 data, *Atmospheric Chemistry and Physics*, *14*(7), 3703–3727, doi:10.5194/acp-14-3703-2014.

Deutscher, N. M., et al. (2014), Drivers of column-average CO2 variability at Southern Hemispheric total carbon column observing network sites, *Atmospheric Chemistry and Physics*, *14*, 9883–9901, doi:10.5194/acp-14-9883-2014.

Dohe, S., V. Sherlock, F. Hase, M. Gisi, J. Robinson, E. Sepúlveda, M. Schneider, and T. Blumenstock (2013), A method to correct sampling ghosts in historic near-infrared Fourier transform spectrometer (FTS) measurements, *Atmospheric Measurement Techniques*, *6*(8), 1981–1992, doi:10.5194/amt-6-1981-2013.

Frankenberg, C., D. Wunch, G. C. Toon, C. Risi, R. A. Scheepmaker, J.-E. Lee, P. O. Wennberg, and J. Worden (2013), Water vapor isotopologue retrievals from high-resolution GOSAT shortwave infrared spectra, *Atmospheric Measurement Techniques*, *6*(2), 263–274, doi:10.5194/amt-6-263-2013.

Fraser, A., et al. (2013), Estimating regional methane surface fluxes: the relative importance of surface and GOSAT mole fraction measurements, *Atmospheric Chemistry and Physics*, *13*(11), 5697–5713, doi:10.5194/acp-13-5697-2013.

Galli, A., et al. (2012), CH4, CO, and H2O spectroscopy for the Sentinel-5 Precursor mission: an assessment with the Total Carbon Column Observing Network measurements, *Atmospheric Measurement Techniques*, *5*(6), 1387–1398, doi:10.5194/amt-5-1387-2012.

Geibel, M. C., et al. (2012), Calibration of column-averaged CH4 over European TCCON FTS sites with airborne in-situ measurements, *Atmospheric Chemistry and Physics*, *12*, 8763–8775, doi:10.5194/acp-12-8763-2012.

Gordon, I. E., S. Kassi, A. Campargue, and G. C. Toon (2010), First identification of the electric quadrupole transitions of oxygen in solar and laboratory spectra, *Journal of Quantitative Spectroscopy and Radiative Transfer*, *111*(9), 1174–1183, doi:10.1016/j.jqsrt.2010.01.008.

Gordon, I. E., L. S. Rothman, and G. C. Toon (2011), Revision of spectral parameters for the B- and γ-bands of oxygen and their validation against atmospheric spectra, *Journal of Quantitative Spectroscopy and Radiative Transfer*, *112*(14), 2310–2322, doi:10.1016/j.jqsrt.2011.05.007.

Guerlet, S., S. Basu, A. Butz, M. Krol, P. Hahne, S. Houweling, O. P. Hasekamp, and I. Aben (2013), Reduced carbon uptake during the 2010 Northern Hemisphere summer from GOSAT, *Geophysical Research Letters*, *40*, 2378–2383, doi:10.1002/grl.50402.

Hamazaki, T. (2005), Fourier transform spectrometer for Greenhouse Gases Observing Satellite (GOSAT), *Proceedings of SPIE*, *5659*, 73–80, doi:10.1117/12.581198.

Hartmann, J.-M., H. Tran, and G. C. Toon (2009), Influence of line mixing on the retrievals of atmospheric CO2 from spectra in the 1.6 and 2.1 μm regions, *Atmospheric Chemistry and Physics*, *9*(19), 7303–7312, doi:10.5194/acp-9-7303-2009.

Houweling, S., et al. (2010), The importance of transport model uncertainties for the estimation of CO2 sources and sinks using satellite measurements, *Atmospheric Chemistry and Physics*, *10*(20), 9981–9992, doi:10.5194/acp-10-9981-2010.

Irion, F. W., et al. (2002), Atmospheric Trace Molecule Spectroscopy (ATMOS) Experiment Version 3 data retrievals, *Applied Optics*, *41*(33), 6968, doi:10.1364/AO.41.006968.

Kalnay, E., et al. (1996), The NCEP/NCAR 40-Year Reanalysis Project, *Bulletin of the American Meteorological Society*, *77*(3), 437–471, doi:10.1175/1520-0477(1996)077⟨0437:TNYRP⟩2.0.CO;2.

Karion, A., C. Sweeney, P. Tans, and T. Newberger (2010), AirCore: An Innovative Atmospheric Sampling System, *Journal of Atmospheric and Oceanic Technology*, *27*(11), 1839–1853, doi:10.1175/2010JTECHA1448.1.

Keppel-Aleks, G., G. C. Toon, P. O. Wennberg, and N. M. Deutscher (2007), Reducing the impact of source brightness fluctuations on spectra obtained by Fourier-transform spectrometry., *Applied Optics*, *46*(21), 4774–9, doi:10.1364/AO.46.004774.

Keppel-Aleks, G., P. O. Wennberg, and T. Schneider (2011), Sources of variations in total column carbon dioxide, *Atmospheric Chemistry and Physics*, *11*(8), 3581–3593, doi:10.5194/acp-11-3581-2011.

Keppel-Aleks, G., et al. (2012), The imprint of surface fluxes and transport on variations in total column carbon dioxide, *Biogeosciences*, *9*(3), 875–891, doi:10.5194/bg-9-875-2012.

Keppel-Aleks, G., et al. (2013), Atmospheric Carbon Dioxide Variability in the Community Earth System Model: Evaluation and Transient Dynamics during the Twentieth and Twenty-First Centuries, *Journal of Climate*, *26*(13), 4447–4475, doi:10.1175/JCLI-D-12-00589.1.

Kurucz, R. L. (2005), The Solar Irradiance by Computation, `http://kurucz.harvard.edu/sun.html`.

Kurucz, R. L. (2008), High Resolution Irradiance Spectra 1560-1720 and 1920-2100 nm, `http://kurucz.harvard.edu/sun/irradiance2008/`.

Kuze, A., H. Suto, M. Nakajima, and T. Hamazaki (2009), Thermal and near infrared sensor for carbon observation Fourier-transform spectrometer on the Greenhouse Gases Observing Satellite for greenhouse gases monitoring., *Applied optics*, *48*(35), 6716–6733, doi:10.1364/AO.48.006716.

Long, D. A., and J. T. Hodges (2012), On spectroscopic models of the O 2 A -band and their impact upon atmospheric retrievals, *Journal of Geophysical Research*, *117*(D12), D12,309, doi:10.1029/2012JD017807.

Mertz, L. (1967), Auxiliary computation for Fourier spectrometry, *Infrared Physics*, *7*(1), 17–23, doi:10.1016/0020-0891(67)90026-7.

Messerschmidt, J., R. Macatangay, J. Notholt, C. Petri, T. Warneke, and C. Weinzierl (2010), Side by side measurements of CO2 by ground-based Fourier transform spectrometry (FTS), *Tellus B*, *62*(5), 749–758, doi:10.1111/j.1600-0889.2010.00491.x.

Messerschmidt, J., et al. (2011), Calibration of TCCON column-averaged CO2: the first aircraft campaign over European TCCON sites, *Atmospheric Chemistry and Physics*, *11*(21), 10,765–10,777, doi:10.5194/acp-11-10765-2011.

Messerschmidt, J., N. Parazoo, D. Wunch, N. M. Deutscher, C. Roehl, T. Warneke, and P. O. Wennberg (2013), Evaluation of seasonal atmosphere-biosphere exchange estimations with TCCON measurements, *Atmospheric Chemistry and Physics*, *13*(10), 5103–5115, doi:10.5194/acp-13-5103-2013.

Miller, C. E., and D. Wunch (2012), Fourier transform spectrometer remote sensing of O2 A-band electric quadrupole transitions, *Journal of Quantitative Spectroscopy and Radiative Transfer*, pp. 1–8, doi:10.1016/j.jqsrt.2012.01.002.

Morino, I., et al. (2011), Preliminary validation of column-averaged volume mixing ratios of carbon dioxide and methane retrieved from GOSAT short-wavelength infrared spectra, *Atmospheric Measurement Techniques*, *4*(6), 1061–1076, doi:10.5194/amt-4-1061-2011.

Mu, M., et al. (2011), Daily and 3-hourly variability in global fire emissions and consequences for atmospheric model predictions of carbon monoxide, *Journal of Geophysical Research*, *116*(D24), D24,303, doi:10.1029/2011JD016245.

Oshchepkov, S., et al. (2013), Simultaneous retrieval of atmospheric CO_2 and light path modification from space-based spectroscopic observations of greenhouse gases: methodology and application to GOSAT measurements over TCCON sites, *Applied Optics*, *52*(6), 1339, doi:10.1364/AO.52.001339.

Pan, L. L., et al. (2010), The Stratosphere-Troposphere Analyses of Regional Transport 2008 Experiment, *Bulletin of the American Meteorological Society*, *91*(3), 327–342, doi:10.1175/2009BAMS2865.1.

Parker, R., et al. (2011), Methane observations from the Greenhouse Gases Observing SATellite: Comparison to ground-based TCCON data and model calculations, *Geophysical Research Letters*, *38*(15), 2–7, doi:10.1029/2011GL047871.

Reuter, M., et al. (2011), Retrieval of atmospheric CO 2 with enhanced accuracy and precision from SCIAMACHY: Validation with FTS measurements and comparison with model results, *Journal of Geophysical Research*, *116*(D4), 1–13, doi:10.1029/2010JD015047.

Reuter, M., et al. (2012), On the potential of the 2041–2047nm spectral region for remote sensing of atmospheric CO2 isotopologues, *Journal of Quantitative Spectroscopy and Radiative Transfer*, *113*(16), 2009–2017, doi:10.1016/j.jqsrt.2012.07.013.

Reuter, M., et al. (2013), A joint effort to deliver satellite retrieved atmospheric CO2 concentrations for surface flux inversions: the ensemble median algorithm EMMA, *Atmospheric Chemistry and Physics*, *13*(4), 1771–1780, doi:10.5194/acp-13-1771-2013.

Rothman, L., et al. (2013), The HITRAN2012 molecular spectroscopic database, *Journal of Quantitative Spectroscopy and Radiative Transfer*, *130*, 4–50, doi:10.1016/j.jqsrt.2013.07.002.

Scheepmaker, R. A., et al. (2013), Improved water vapour spectroscopy in the 4174–4300 cm^{-1} region and its impact on SCIAMACHY HDO/H2O measurements, *Atmospheric Measurement Techniques*, *6*(4), 879–894, doi:10.5194/amt-6-879-2013.

Schepers, D., et al. (2012), Methane retrievals from Greenhouse Gases Observing Satellite (GOSAT) shortwave infrared measurements: Performance comparison of proxy and physics retrieval algorithms, *Journal of Geophysical Research*, *117*(D10), 1–14, doi:10.1029/2012JD017549.

Schneising, O., et al. (2012), Atmospheric greenhouse gases retrieved from SCIAMACHY: comparison to ground-based FTS measurements and model results, *Atmospheric Chemistry and Physics*, *12*(3), 1527–1540, doi:10.5194/acp-12-1527-2012.

Singh, H. B., W. H. Brune, J. H. Crawford, D. J. Jacob, and P. B. Russell (2006), Overview of the summer 2004 Intercontinental Chemical Transport Experiment-North America (INTEX-A), *Journal of Geophysical Research: Atmospheres*, *111*(24), doi:10.1029/2006JD007905.

Sussmann, R., F. Forster, M. Rettinger, and P. Bousquet (2012), Renewed methane increase for five years (2007–2011) observed by solar FTIR spectrometry, *Atmospheric Chemistry and Physics*, *12*(11), 4885–4891, doi:10.5194/acp-12-4885-2012.

Thompson, D. R., et al. (2012), Atmospheric validation of high accuracy CO2 absorption coefficients for the OCO-2 mission, *Journal of Quantitative Spectroscopy and Radiative Transfer*, *113*, 2265–2276, doi:10.1016/j.jqsrt.2012.05.021.

Thuillier, G., M. Hersé, D. Labs, T. Foujols, W. Peetermans, D. Gillotay, P. C. Simon, and H. Mandel (2003), The solar spectral irradiance from 200 to 2400 nm as measured by the SOLSPEC spectrometer from the ATLAS and EURECA missions, *Solar Physics*, *214*(1), 1–22, doi:10.1023/A:1024048429145.

Toon, G. C. (1991), The JPL MkIV interferometer, *Optics and Photonics News*, *2*(10), 19, doi:10.1364/OPN.2.10.000019.

Toon, G. C. (2014a), Telluric line list for GGG2014, TCCON data archive, hosted by the Carbon Dioxide Information Analysis Center, Oak Ridge National Laboratory, Oak Ridge, Tennessee, U.S.A., doi:10.14291/tccon.ggg2014.atm.R0/1221656.

Toon, G. C. (2014b), Solar line list for GGG2014, TCCON data archive, hosted by the Carbon Dioxide Information Analysis Center, Oak Ridge National Laboratory, Oak Ridge, Tennessee, U.S.A., doi:10.14291/tccon.ggg2014.solar.R0/1221658.

Toon, G. C., and D. Wunch (2014), A stand-alone a priori profile generation tool for GGG2014, TCCON data archive, hosted by the Carbon Dioxide Information Analysis Center, Oak Ridge National Laboratory, Oak Ridge, Tennessee, U.S.A., doi:10.14291/tccon.ggg2014.priors.R0/1221661.

Tran, H., and J.-M. Hartmann (2008), An improved O2 A band absorption model and its consequences for retrievals of photon paths and surface pressures, *Journal of Geophysical Research*, *113*(D18), 1–10, doi:10.1029/2008JD010011.

Tran, H., J.-M. Hartmann, G. C. Toon, L. Brown, C. Frankenberg, T. Warneke, P. Spietz, and F. Hase (2010), The $2\nu 3$ band of CH4 revisited with line mixing: Consequences for spectroscopy and atmospheric retrievals at 1.67μm, *Journal of Quantitative Spectroscopy and Radiative Transfer*, *111*(10), 1344–1356, doi:10.1016/j.jqsrt.2010.02.015.

Wallace, L., and W. Livingston (2003), *An atlas of the solar spectrum in the infrared from 1850 to 9000 cm-1 (1.1 to 5.4 micrometer)*.

Washenfelder, R. A., G. C. Toon, J.-F. L. Blavier, Z. Yang, N. T. Allen, P. O. Wennberg, S. A. Vay, D. M. Matross, and B. C. Daube (2006), Carbon dioxide column abundances at the Wisconsin Tall Tower site, *Journal of Geophysical Research*, *111*(D22), 1–11, doi:10.1029/2006JD007154.

Wofsy, S. C. (2011), HIAPER Pole-to-Pole Observations (HIPPO): fine-grained, global-scale measurements of climatically important atmospheric gases and aerosols., *Philosophical Transactions of the Royal Society - Series A: Mathematical, Physical and Engineering Sciences*, *369*(1943), 2073–86, doi:10.1098/rsta.2010.0313.

Wunch, D., et al. (2010), Calibration of the Total Carbon Column Observing Network using aircraft profile data, *Atmospheric Measurement Techniques*, *3*(5), 1351–1362, doi:10.5194/amt-3-1351-2010.

Wunch, D., et al. (2011a), A method for evaluating bias in global measurements of CO2 total columns from space, *Atmospheric Chemistry and Physics*, *11*(23), 12,317–12,337, doi:10.5194/acp-11-12317-2011.

Wunch, D., G. C. Toon, J.-F. L. Blavier, R. A. Washenfelder, J. Notholt, B. J. Connor, D. W. T. Griffith, V. Sherlock, and P. O. Wennberg (2011b), The total carbon column observing network, *Philosophical Transactions of the Royal Society - Series A: Mathematical, Physical and Engineering Sciences*, *369*(1943), 2087–2112, doi:10.1098/rsta.2010.0240.

Wunch, D., et al. (2013), The covariation of Northern Hemisphere summertime CO2 with surface temperature in boreal regions, *Atmospheric Chemistry and Physics*, *13*(18), 9447–9459, doi:10.5194/acp-13-9447-2013.

Table 1: A chronological list of sites currently in operation. The Data Reference includes a DOI. The DOI naming convention is 10.14291/tccon.ggg2014.SiteName.version/unique, where the version is the data revision number (e.g., R0 for initial versions, R1 for a superseding version, etc.), and each site has an unique suffix identifier.

Site Location SiteName	Latitude, Longitude, Altitude (km)	Start Date	Data Reference
Park Falls, WI, USA parkfalls01	45.94°N, 90.27°W 0.44	2004/05/26	Wennberg, P. O., C. Roehl, D. Wunch, G. C. Toon, J.-F. Blavier, R. Washenfelder, G. Keppel-Aleks, N. Allen, J. Ayers. 2014. TCCON data from Park Falls, Wisconsin, USA, Release GGG2014R0. TCCON data archive, hosted by the Carbon Dioxide Information Analysis Center, Oak Ridge National Laboratory, Oak Ridge, Tennessee, U.S.A. DOI: 10.14291/tccon.ggg2014.parkfalls01.R0/1149161
Ny-Ålesund, Norway nyalesund01	78.92°N, 11.92°E 0.02	2005/03/14	Notholt, J., O. Schrems, T. Warneke, N. Deutscher, C. Weinzierl, M. Palm, M. Buschmann, AWI-PEV Station Engineers. 2014. TCCON data from Ny Alesund, Spitzbergen, Norway, Release GGG2014R0. TCCON data archive, hosted by the Carbon Dioxide Information Analysis Center, Oak Ridge National Laboratory, Oak Ridge, Tennessee, U.S.A. DOI: 10.14291/tccon.ggg2014.nyalesund01.R0/1149278
Darwin, Australia darwin01	12.43°S, 130.89°E 0.03	2005/08/28	Griffith, D. W. T., N. Deutscher, V. A. Velazco, P. O. Wennberg, Y. Yavin, G. Keppel Aleks, R. Washenfelder, G. C. Toon, J.-F. Blavier, C. Murphy, N. Jones, G. Kettlewell, B. Connor, R. Macatangay, C. Roehl, M. Ryczek, J. Glowacki, T. Culgan, G. Bryant. 2014. TCCON data from Darwin, Australia, Release GGG2014R0. TCCON data archive, hosted by the Carbon Dioxide Information Analysis Center, Oak Ridge National Laboratory, Oak Ridge, Tennessee, U.S.A. DOI: 10.14291/tccon.ggg2014.darwin01.R0/1149290
Bremen, Germany bremen01	53.1037°N, 8.849517°E 0.03	2006/01/01	Notholt, J., C. Petri, T. Warneke, N. Deutscher, M. Buschmann, C. Weinzierl, R. Macatangay, P. Grupe. 2014. TCCON data from Bremen, Germany, Release GGG2014R0. TCCON data archive, hosted by the Carbon Dioxide Information Analysis Center, Oak Ridge National Laboratory, Oak Ridge, Tennessee, U.S.A. DOI: 10.14291/tccon.ggg2014.bremen01.R0/1149275
Izaña, Tenerife, Spain izana01	28.3°N, 16.48°W 2.37	2007/05/18	Blumenstock, T., F. Hase, M. Schneider, O.E. García, E. Sepúlveda. 2014. TCCON data from Izana, Tenerife, Spain, Release GGG2014R0. TCCON data archive, hosted by the Carbon Dioxide Information Analysis Center, Oak Ridge National Laboratory, Oak Ridge, Tennessee, U.S.A. DOI: 10.14291/tccon.ggg2014.izana01.R0/1149295

Site Location SiteName	Latitude, Longitude, Altitude (km)	Start Date	Data Reference
Garmisch, Germany garmisch01	47.48°N, 11.06°E 0.75	2007/07/16	Sussmann, R., M. Rettinger. 2014. TCCON data from Garmisch, Germany, Release GGG2014R0. TCCON data archive, hosted by the Carbon Dioxide Information Analysis Center, Oak Ridge National Laboratory, Oak Ridge, Tennessee, U.S.A. DOI: 10.14291/tccon.ggg2014.garmisch01.R0/1149299
Wollongong, Australia wollongong01	34.41°S, 150.88°E 0.03	2008/06/26	Griffith, D. W. T., V. A. Velazco, N. Deutscher, C. Murphy, N. Jones, S. Wilson, R. Macatangay, G. Kettlewell, R. R. Buchholz, M. Riggenbach. 2014. TCCON data from Wollongong, Australia, Release GGG2014R0. TCCON data archive, hosted by the Carbon Dioxide Information Analysis Center, Oak Ridge National Laboratory, Oak Ridge, Tennessee, U.S.A. DOI: 10.14291/tccon.ggg2014.wollongong01.R0/1149291
Lamont, OK, USA lamont01	36.6°N, 97.49°W 0.32	2008/07/06	Wennberg, P. O., D. Wunch, C. Roehl, J.-F. Blavier, G. C. Toon, N. Allen, P. Dowell, K. Teske, C. Martin, J. Martin. 2014. TCCON data from Lamont, Oklahoma, USA, Release GGG2014R0. TCCON data archive, hosted by the Carbon Dioxide Information Analysis Center, Oak Ridge National Laboratory, Oak Ridge, Tennessee, U.S.A. DOI: 10.14291/tccon.ggg2014.lamont01.R0/1149159
Białystok, Poland bialystok01	53.23°N, 23.02°E 0.13	2009/03/13	Deutscher, N., J. Notholt, J. Messerschmidt, C. Weinzierl, T. Warneke, C. Petri, P. Grupe, K. Katrynski. 2014. TCCON data from Bialystok, Poland, Release GGG2014R1. TCCON data archive, hosted by the Carbon Dioxide Information Analysis Center, Oak Ridge National Laboratory, Oak Ridge, Tennessee, U.S.A. DOI: 10.14291/tccon.ggg2014.bialystok01.R1/1183984
Sodankylä, Finland sodankyla01	67.37°N, 26.63°E 0.19	2009/05/16	Kivi, R., P. Heikkinen, E. Kyro. 2014. TCCON data from Sodankyla, Finland, Release GGG2014R0. TCCON data archive, hosted by the Carbon Dioxide Information Analysis Center, Oak Ridge National Laboratory, Oak Ridge, Tennessee, U.S.A. DOI: 10.14291/tccon.ggg2014.sodankyla01.R0/1149280
Orléans, France orleans01	47.97°N, 2.11°E 0.13	2009/08/29	Warneke, T., J. Messerschmidt, J. Notholt, C. Weinzierl, N. Deutscher, C. Petri, P. Grupe, C. Vuillemin, F. Truong, M. Schmidt, M. Ramonet, E. Parmentier. 2014. TCCON data from Orleans, France, Release GGG2014R0. TCCON data archive, hosted by the Carbon Dioxide Information Analysis Center, Oak Ridge National Laboratory, Oak Ridge, Tennessee, U.S.A. DOI: 10.14291/tccon.ggg2014.orleans01.R0/1149276

Site Location SiteName	Latitude, Longitude, Altitude (km)	Start Date	Data Reference
Lauder, New Zealand, 125HR lauder02	45.04°S, 169.68°E 0.37	2010/02/02	Sherlock, V., B. Connor, J. Robinson, H. Shiona, D. Smale, D. Pollard. 2014. TCCON data from Lauder, New Zealand, 125HR, Release GGG2014R0. TCCON data archive, hosted by the Carbon Dioxide Information Analysis Center, Oak Ridge National Laboratory, Oak Ridge, Tennessee, U.S.A. DOI: 10.14291/tccon.ggg2014.lauder02.R0/1149298
Karlsruhe, Germany karlsruhe01	49.1°N, 8.44°E 0.11	2010/04/19	Hase, F., T. Blumenstock, S. Dohe, J. Groß, M. Kiel. 2014. TCCON data from Karlsruhe, Germany, Release GGG2014R1. TCCON data archive, hosted by the Carbon Dioxide Information Analysis Center, Oak Ridge National Laboratory, Oak Ridge, Tennessee, U.S.A. DOI: 10.14291/tccon.ggg2014.karlsruhe01.R1/1182416
Eureka, Canada eureka01	80.05°N, 86.42°W 0.61	2010/07/24	Strong, K., J. Mendonca, D. Weaver, P. Fogal, J.R. Drummond, R. Batchelor, R. Lindenmaier. 2014. TCCON data from Eureka, Canada, Release GGG2014R0. TCCON data archive, hosted by the Carbon Dioxide Information Analysis Center, Oak Ridge National Laboratory, Oak Ridge, Tennessee, U.S.A. DOI: 10.14291/tccon.ggg2014.eureka01.R0/1149271
Saga, Japan saga01	33.24°N, 130.29°E 0.01	2011/07/28	Shiomi, K., Kawakami, S., H. Ohyama, K. Arai, H. Okumura, C. Taura, T. Fukamachi, M. Sakashita. 2014. TCCON data from Saga, Japan, Release GGG2014R0. TCCON data archive, hosted by the Carbon Dioxide Information Analysis Center, Oak Ridge National Laboratory, Oak Ridge, Tennessee, U.S.A. DOI: 10.14291/tccon.ggg2014.saga01.R0/1149283
Tsukuba, Japan, 125HR tsukuba02	36.05°N, 140.12°E 0.03	2011/08/04	Morino, I., T. Matsuzaki, A. Shishime. 2014. TCCON data from Tsukuba, Ibaraki, Japan, 125HR, Release GGG2014R0. TCCON data archive, hosted by the Carbon Dioxide Information Analysis Center, Oak Ridge National Laboratory, Oak Ridge, Tennessee, U.S.A. DOI: 10.14291/tccon.ggg2014.tsukuba02.R0/1149301
Île de La Réunion, France reunion01	20.9°S, 55.49°E 0.09	2011/09/16	De Maziere, M., M. K. Sha, F. Desmet, C. Hermans, F. Scolas, N. Kumps, J.-M. Metzger, V. Duflot, J.-P. Cammas. 2014. TCCON data from Reunion Island (La Reunion), France, Release GGG2014R0. TCCON data archive, hosted by the Carbon Dioxide Information Analysis Center, Oak Ridge National Laboratory, Oak Ridge, Tennessee, U.S.A. DOI: 10.14291/tccon.ggg2014.reunion01.R0/1149288

Site Location SiteName	Latitude, Longitude, Altitude (km)	Start Date	Data Reference
Ascension Island, Saint Helena ascension01	7.92°S, 14.33°W 0.03	2012/05/22	Feist, D. G., S. G. Arnold, N. John, M. C. Geibel. 2014. TCCON data from Ascension Island, Saint Helena, Ascension and Tristan da Cunha, Release GGG2014R0. TCCON data archive, hosted by the Carbon Dioxide Information Analysis Center, Oak Ridge National Laboratory, Oak Ridge, Tennessee, U.S.A. DOI: 10.14291/tccon.ggg2014.ascension01.R0/1149285
Caltech, Pasadena, CA, USA pasadena01	34.14°N, 118.13°W 0.24	2012/09/20	Wennberg, P. O., D. Wunch, C. Roehl , J.-F. Blavier, G. C. Toon, N. Allen. 2014. TCCON data from California Institute of Technology, Pasadena, California, USA, Release GGG2014R1. TCCON data archive, hosted by the Carbon Dioxide Information Analysis Center, Oak Ridge National Laboratory, Oak Ridge, Tennessee, U.S.A. DOI: 10.14291/tccon.ggg2014.pasadena01.R1/1182415
Edwards, CA, USA edwards01	34.96°N, 117.88°W 0.7	2013/07/20	Iraci, L., J. Podolske, P. Hillyard, C. Roehl, P. O. Wennberg, J.-F. Blavier, J. Landeros, N. Allen, D. Wunch, J. Zavaleta, E. Quigley, G. Osterman, R. Albertson, K. Dunwoody, H. Boyden. 2014. TCCON data from Armstrong Flight Research Center, Edwards, CA, USA, Release GGG2014R0. TCCON data archive, hosted by the Carbon Dioxide Information Analysis Center, Oak Ridge National Laboratory, Oak Ridge, Tennessee, U.S.A. DOI: 10.14291/tccon.ggg2014.edwards01.R0/1149289
Rikubetsu, Japan rikubetsu01	43.46°N, 143.77°E 0.38	2013/11/16	Morino, I., N. Yokozeki, T. Matzuzaki, A. Shishime. 2014. TCCON data from Rikubetsu, Hokkaido, Japan, Release GGG2014R0. TCCON data archive, hosted by the Carbon Dioxide Information Analysis Center, Oak Ridge National Laboratory, Oak Ridge, Tennessee, U.S.A. DOI: 10.14291/tccon.ggg2014.rikubetsu01.R0/1149282
Paris, France paris01	48.85°N, 2.36°E 0.06	2014/09/23	Te, Y., P. Jeseck, C. Janssen. 2014. TCCON data from Paris, France, Release GGG2014R0. TCCON data archive, hosted by the Carbon Dioxide Information Analysis Center, Oak Ridge National Laboratory, Oak Ridge, Tennessee, U.S.A. DOI: 10.14291/tccon.ggg2014.paris01.R0/1149279

Table 2: A list of sites previously in operation, with instruments that have since moved to new locations, or have been replaced by newer models. The lauder01 (120HR) instrument was replaced by the lauder02 (125HR) instrument. The other sites were moved to new locations. The jpl02 instrument was also located in Indianapolis and Edwards.

Site Location SiteName	Latitude, Longitude Altitude (km)	Start Date End Date	New Location(s)	Data Reference
Lauder, New Zealand, 120HR lauder01	45.05°S, 169.68°E 0.37	2004/06/29 2010/12/09	lauder02	Sherlock, V., B. Connor, J. Robinson, H. Shiona, D. Smale, D. Pollard. 2014. TCCON data from Lauder, New Zealand, 120HR, Release GGG2014R0. TCCON data archive, hosted by the Carbon Dioxide Information Analysis Center, Oak Ridge National Laboratory, Oak Ridge, Tennessee, U.S.A. DOI: 10.14291/tccon.ggg2014.lauder01.R0/1149293
JPL, Pasadena, CA, USA jpl01	34.2°N, 118.18°W 0.39	2007/07/31 2008/06/22	lamont01	Wennberg, P. O., D. Wunch, Y. Yavin, G. C. Toon, J.-F. Blavier, N. Allen, G. Keppel-Aleks. 2014. TCCON data from Jet Propulsion Laboratory, Pasadena, California, USA, Release GGG2014R0. TCCON data archive, hosted by the Carbon Dioxide Information Analysis Center, Oak Ridge National Laboratory, Oak Ridge, Tennessee, U.S.A. DOI: 10.14291/tccon.ggg2014.jpl01.R0/1149163
Tsukuba, Japan, 120HR tsukuba01	36.05°N, 140.12°E 0.03	2008/12/25 2010/03/22	rikubetsu01	Morino, I., T. Matsuzaki, A. Shishime. 2014. TCCON data from Tsukuba, Ibaraki, Japan, 120HR, Release GGG2014R0. TCCON data archive, hosted by the Carbon Dioxide Information Analysis Center, Oak Ridge National Laboratory, Oak Ridge, Tennessee, U.S.A. DOI: 10.14291/tccon.ggg2014.tsukuba01.R0/1149281
Four Corners, NM, USA fourcorners01	36.8°N, 108.48°W 1.64	2011/03/10 2013/01/20	manaus01	Dubey, M., R. Lindenmaier, B. Henderson, D. Green, N. Allen, C. Roehl, J.-F. Blavier, Z. Butterfield, S. Love, J. Hamelmann, D. Wunch. 2014. TCCON data from Four Corners, NM, USA, Release GGG2014R0. TCCON data archive, hosted by the Carbon Dioxide Information Analysis Center, Oak Ridge National Laboratory, Oak Ridge, Tennessee, U.S.A. DOI: 10.14291/tccon.ggg2014.fourcorners01.R0/1149272
JPL, Pasadena, CA, USA jpl02	34.2°N, 118.18°W 0.39	2011/05/19 2013/07/01	indianapolis01, edwards01	Wennberg, P. O., C. Roehl, J.-F. Blavier, D. Wunch, J. Landeros, N. Allen. 2014. TCCON data from Jet Propulsion Laboratory, Pasadena, California, USA, Release GGG2014R0. TCCON data archive, hosted by the Carbon Dioxide Information Analysis Center, Oak Ridge National Laboratory, Oak Ridge, Tennessee, U.S.A. DOI: 10.14291/tccon.ggg2014.jpl02.R0/1149297
Indianapolis, IN, USA indianapolis01	39.86°N, 86°W 0.27	2012/08/23 2012/12/01	jpl02, edwards01	Iraci, L., J. Podolske, P. Hillyard, C. Roehl, P. O. Wennberg, J.-F. Blavier, J. Landeros, N. Allen, D. Wunch, J. Zavaleta, E. Quigley, G. Osterman, E. Barrow, J. Barney. 2014. TCCON data from Indianapolis, Indiana, USA, Release GGG2014R0. TCCON data archive, hosted by the Carbon Dioxide Information Analysis Center, Oak Ridge National Laboratory, Oak Ridge, Tennessee, U.S.A. DOI: 10.14291/tccon.ggg2014.indianapolis01.R0/1149164
Manaus, Brazil manaus01	3.21°S, 60.6°W 0.05	2014/10/01 2015/07/31		Dubey, M., B. Henderson, D. Green, Z. Butterfield, G. Keppel-Aleks, N. Allen, J.-F. Blavier, C. Roehl, D. Wunch, R. Lindenmaier. 2014. TCCON data from Manaus, Brazil, Release GGG2014R0. TCCON data archive, hosted by the Carbon Dioxide Information Analysis Center, Oak Ridge National Laboratory, Oak Ridge, Tennessee, U.S.A. DOI: 10.14291/tccon.ggg2014.manaus01.R0/1149274

Table 3: Retrieval Windows

Target Gas	Central Wavenumber (cm^{-1})	Window Width (cm^{-1})	Interfering Species
CO_2	6220.00	80.00	H_2O, HDO, CH_4
	6339.50	85.00	H_2O, HDO
CH_4	5938.00	116.00	CO_2, H_2O, N_2O
	6002.00	11.10	CO_2, H_2O, HDO
	6076.00	138.00	CO_2, H_2O, HDO
CO	4233.00	48.60	CH_4, H_2O, HDO
	4290.40	56.80	CH_4, H_2O, HDO
N_2O	4395.20	43.40	CH_4, H_2O, HDO
	4430.10	23.10	CH_4, H_2O, HDO, CO_2
	4719.50	73.10	CH_4, H_2O, CO_2
O_2	7885.00	240.00	O_2 continuum, H_2O, HF, CO_2
HF	4038.95	0.32	H_2O
HDO	4054.60	3.30	H_2O, CH_4
	4116.10	8.00	H_2O, CH_4
	4212.45	1.90	H_2O, CH_4
	4232.50	11.00	H_2O, CH_4, CO
	6330.05	45.50	H_2O, CO_2
	6377.40	50.20	H_2O, CO_2
H_2O	4565.20	2.50	CO_2, CH_4
	4571.75	2.50	
	4576.85	1.90	CH_4
	4611.05	2.20	CH_4
	4622.00	2.30	CO_2
	4699.55	4.00	CO_2, N_2O
	6076.90	3.85	CH_4, HDO, CO_2
	6099.35	0.95	HDO, CO_2
	6125.85	1.45	HDO, CO_2, CH_4
	6177.30	0.83	HDO, CO_2, CH_4
	6255.95	3.60	CO_2, HDO
	6301.35	7.90	CO_2, HDO
	6392.45	3.10	HDO
	6401.15	1.15	HDO, CO_2
	6469.60	3.50	CO_2, HDO

Table 4: GGG2014 correction factors and the GGG2012 correction factors for comparison. Uncertainties on the airmass-dependent correction factors (ADCF) are 1-σ standard deviations which represent day-to-day variability. This vastly overestimates the uncertainty in the average value (based on thousands of observations). Unfortunately, the standard error underestimates the uncertainties, because the airmass-dependent correction factors may not be constant over time (e.g., due to instrumental drifts). Uncertainties on the airmass independent correction factors (AICF) are 2-σ errors on the best fit line. The error on the N_2O AICF is larger in GGG2014 than in GGG2012 because of an additional site (Four Corners) that was added to the regression.

	GGG2012		GGG2014	
Gas	ADCF	AICF	ADCF	AICF
X_{CO_2}	-0.0065 ± 0.0050	0.989 ± 0.001	-0.0068 ± 0.0050	0.9898 ± 0.0010
X_{CH_4}	$+0.0055 \pm 0.0080$	0.978 ± 0.002	$+0.0053 \pm 0.0080$	0.9765 ± 0.0020
X_{N_2O}	$+0.0172 \pm 0.0100$	0.958 ± 0.005	$+0.0039 \pm 0.0100$	0.9638 ± 0.0100
X_{CO}	N/A	0.98 ± 0.02	-0.0483 ± 0.1000	1.0672 ± 0.0200
X_{H_2O}	N/A	1.031 ± 0.01	N/A	1.0183 ± 0.0100

Table 5: CO_2 *in situ* profiles measured above TCCON stations.

TCCON Site	Airborne Measurement	Date and Time	Floor, Ceiling Altitude (m)
Park Falls	INTEX-NA DC8	2004-07-12 16:48:13	760.4, 10550.6
Park Falls	INTEX-NA DC8, COBRA King Air	2004-07-15 14:38:56	617.8, 11026.0
Park Falls	INTEX-NA DC8	2004-07-15 17:21:41	637.3, 11026.0
Park Falls	COBRA King Air	2004-08-14 21:19:10	778.1, 9679.3
Park Falls	COBRA King Air	2004-08-15 20:09:08	714.4, 7602.3
Darwin	Proteus	2006-02-04 01:08:19	946.9, 14094.1
Park Falls	START-08 GV	2008-05-12 17:38:54	1198.5, 9350.2
Tsukuba	Beechcraft King Air 200T	2009-01-15 01:50:00	366.3, 6775.6
Lauder	HIPPO GV	2009-01-20 21:50:20	667.0, 14573.0
Lamont	HIPPO GV	2009-01-30 20:46:30	438.1, 13255.8
Lamont	NASA Glenn Lear-25 (5–13 km altitude) and Cessna 210 (0.3–5 km altitude)	2009-07-31 16:01:00	457.2, 11233.4
Lamont	NASA Glenn Lear-25 (5–13 km altitude) and Cessna 210 (0.3–5 km altitude)	2009-08-02 16:30:00	457.2, 12831.8
Lamont	NASA Glenn Lear-25 (5–13 km altitude) and Cessna 210 (0.3–5 km altitude)	2009-08-03 16:40:00	457.2, 12855.5
Bialystok	Enviscope Learjet (IMECC)	2009-09-30 09:51:10	440.4, 11384.4
Bialystok	Enviscope Learjet (IMECC)	2009-09-30 13:56:40	758.2, 10449.7
Orleans	Enviscope Learjet (IMECC)	2009-10-02 06:46:47	607.5, 11395.2
Karlsruhe	Enviscope Learjet (IMECC)	2009-10-02 09:25:46	100.7, 6767.8
Orleans	Enviscope Learjet (IMECC)	2009-10-02 10:42:42	598.4, 11054.7
Jena	Enviscope Learjet (IMECC)	2009-10-05 08:02:53	781.3, 12308.1
Garmisch	Enviscope Learjet (IMECC)	2009-10-05 08:57:45	1409.0, 12618.2
Bremen	Enviscope Learjet (IMECC)	2009-10-05 12:03:27	449.7, 12932.4
Jena	Enviscope Learjet (IMECC)	2009-10-09 10:22:22	424.2, 12617.8
Bremen	Enviscope Learjet (IMECC)	2009-10-09 11:19:28	459.8, 12389.2
Wollongong	HIPPO GV	2009-11-15 00:42:45	109.1, 12562.7
Lamont	Learjet	2010-07-18 18:25:14	410.0, 12932.0
Four Corners	HIPPO GV	2011-06-07 17:57:36	2068.0, 13111.5
Lamont	AirCore	2012-01-14 20:28:50	742.1, 28855.6
Lamont	AirCore	2012-01-14 20:54:52	569.8, 28169.6
Lamont	AirCore	2012-01-15 15:57:41	637.2, 29293.7
Lamont	AirCore	2012-01-15 15:59:24	683.7, 28411.0
Lamont	AirCore	2012-10-23 21:34:49	374.3, 27689.1
Lamont	AirCore	2012-10-24 19:20:00	356.1, 29176.7
Lamont	AirCore	2013-07-23 19:53:46	463.1, 28531.5
Lamont	AirCore	2013-07-23 20:11:00	459.9, 29491.9

Table 6: CH_4 *in situ* profiles measured above TCCON stations.

TCCON Site	Airborne Measurement	Date and Time	Floor, Ceiling Altitude (m)
Park Falls	INTEX-NA DC8	2004-07-12 16:48:14	732.0, 10064.0
Park Falls	START-08 GV	2008-05-12 17:38:54	1198.5, 9350.2
Tsukuba	Beechcraft King Air 200T	2009-01-15 04:06:00	457.8, 6765.6
Lauder	HIPPO GV	2009-01-20 21:50:20	667.0, 14573.0
Lamont	HIPPO GV	2009-01-30 20:46:30	438.1, 12999.7
Lamont	NASA Glenn Lear-25 (5–13 km altitude) and Cessna 210 (0.3–5 km altitude)	2009-07-31 16:01:00	457.2, 11233.4
Lamont	NASA Glenn Lear-25 (5–13 km altitude) and Cessna 210 (0.3–5 km altitude)	2009-08-02 16:30:00	457.2, 12831.8
Lamont	NASA Glenn Lear-25 (5–13 km altitude) and Cessna 210 (0.3–5 km altitude)	2009-08-03 16:40:00	457.2, 12855.5
Bialystok	Enviscope Learjet (IMECC)	2009-09-30 09:51:10	440.4, 11384.4
Bialystok	Enviscope Learjet (IMECC)	2009-09-30 13:56:40	758.2, 10449.7
Orleans	Enviscope Learjet (IMECC)	2009-10-02 06:46:47	607.5, 11395.2
Karlsruhe	Enviscope Learjet (IMECC)	2009-10-02 09:25:46	100.7, 6767.8
Orleans	Enviscope Learjet (IMECC)	2009-10-02 10:42:42	598.4, 11054.7
Jena	Enviscope Learjet (IMECC)	2009-10-05 08:02:53	781.3, 12308.1
Garmisch	Enviscope Learjet (IMECC)	2009-10-05 08:57:45	1409.0, 12618.2
Bremen	Enviscope Learjet (IMECC)	2009-10-05 12:03:27	449.7, 12932.4
Jena	Enviscope Learjet (IMECC)	2009-10-09 10:22:22	424.2, 12617.8
Bremen	Enviscope Learjet (IMECC)	2009-10-09 11:19:28	459.8, 13243.9
Wollongong	HIPPO GV	2009-11-15 00:42:45	109.1, 12562.7
Four Corners	HIPPO GV	2011-06-07 17:56:50	1746.2, 13281.3
Lamont	AirCore	2012-01-14 20:28:50	742.1, 28855.6
Lamont	AirCore	2012-01-14 20:54:52	569.8, 28169.6
Lamont	AirCore	2012-01-15 15:57:41	637.2, 29293.7
Lamont	AirCore	2012-01-15 15:59:24	683.7, 28411.0
Lamont	AirCore	2012-10-23 21:34:49	374.3, 27689.1
Lamont	AirCore	2012-10-24 19:20:00	356.1, 29176.7
Lamont	AirCore	2013-07-23 19:53:46	463.1, 28531.5
Lamont	AirCore	2013-07-23 20:11:00	459.9, 29491.9

Table 7: CO *in situ* profiles measured above TCCON stations.

TCCON Site	Airborne Measurement	Date and Time	Floor, Ceiling Altitude (m)
Park Falls	COBRA King Air	2004-07-15 14:45:45	712.5, 7600.4
Park Falls	COBRA King Air	2004-08-15 20:09:08	714.4, 7602.3
Park Falls	START-08 GV	2008-05-12 17:38:54	1198.5, 9350.2
Lauder	HIPPO GV	2009-01-20 21:50:20	667.0, 14573.0
Lamont	HIPPO GV	2009-01-30 20:46:30	438.1, 12999.7
Lamont	NASA Glenn Lear-25 (5–13 km altitude) and Cessna 210 (0.3–5 km altitude)	2009-07-31 16:01:00	457.2, 11233.4
Lamont	NASA Glenn Lear-25 (5–13 km altitude) and Cessna 210 (0.3–5 km altitude)	2009-08-02 16:30:00	457.2, 12831.8
Lamont	NASA Glenn Lear-25 (5–13 km altitude) and Cessna 210 (0.3–5 km altitude)	2009-08-03 16:40:00	457.2, 12855.5
Bialystok	Enviscope Learjet (IMECC)	2009-09-30 09:51:10	440.4, 11371.1
Bialystok	Enviscope Learjet (IMECC)	2009-09-30 13:56:40	758.2, 10449.7
Orleans	Enviscope Learjet (IMECC)	2009-10-02 06:46:47	693.1, 11395.2
Karlsruhe	Enviscope Learjet (IMECC)	2009-10-02 09:25:46	100.7, 6767.8
Orleans	Enviscope Learjet (IMECC)	2009-10-02 10:42:42	598.4, 11054.7
Jena	Enviscope Learjet (IMECC)	2009-10-05 08:02:53	781.3, 12308.1
Garmisch	Enviscope Learjet (IMECC)	2009-10-05 08:57:45	1409.0, 12618.2
Bremen	Enviscope Learjet (IMECC)	2009-10-05 12:03:27	449.7, 12932.4
Jena	Enviscope Learjet (IMECC)	2009-10-09 10:22:22	424.2, 12617.8
Bremen	Enviscope Learjet (IMECC)	2009-10-09 11:19:28	459.8, 13243.9
Wollongong	HIPPO GV	2009-11-15 00:42:45	109.1, 12562.7
Four Corners	HIPPO GV	2011-06-07 17:56:50	1746.2, 13281.3
Lamont	AirCore	2012-01-14 20:28:50	742.1, 13000.0
Lamont	AirCore	2012-01-14 20:54:52	569.8, 13000.0
Lamont	AirCore	2012-01-15 15:57:41	637.2, 29293.7
Lamont	AirCore	2012-01-15 15:59:24	683.7, 28411.0
Lamont	AirCore	2012-10-24 19:20:00	356.1, 29176.7

Table 8: N_2O *in situ* profiles measured above TCCON stations.

TCCON Site	Airborne Measurement	Date and Time	Floor, Ceiling Altitude (m)
Park Falls	START-08 GV	2008-05-12 17:38:54	1198.5, 9350.2
Lauder	HIPPO GV	2009-01-20 21:50:20	667.0, 14573.0
Lamont	HIPPO GV	2009-01-30 20:46:30	438.1, 12999.7
Lamont	NASA Glenn Lear-25 (5–13 km altitude) and Cessna 210 (0.3–5 km altitude)	2009-07-31 16:01:00	457.2, 11233.4
Lamont	NASA Glenn Lear-25 (5–13 km altitude) and Cessna 210 (0.3–5 km altitude)	2009-08-02 16:30:00	457.2, 12831.8
Lamont	NASA Glenn Lear-25 (5–13 km altitude) and Cessna 210 (0.3–5 km altitude)	2009-08-03 16:40:00	457.2, 12855.5
Wollongong	HIPPO GV	2009-11-15 00:42:45	109.1, 12562.7
Four Corners	HIPPO GV	2011-06-07 17:56:50	1746.2, 13281.3

Table 9: H_2O *in situ* profiles measured above TCCON stations.

TCCON Site	Airborne Measurement	Date and Time	Floor, Ceiling Altitude (m)
Darwin	Radiosonde RS92-15 Vaisala	2006-02-02 05:17:00	30.0, 29319.0
Darwin	Radiosonde RS92-15 Vaisala	2006-02-02 23:15:00	30.0, 32912.0
Darwin	Radiosonde RS92-15 Vaisala	2006-02-03 05:17:00	30.0, 27540.0
Darwin	Radiosonde RS92-15 Vaisala	2006-02-03 23:15:00	30.0, 32778.0
Darwin	Radiosonde RS92-15 Vaisala	2006-02-04 05:15:00	30.0, 28354.0
Tsukuba	Radiosonde RS2-91 Meisei Electric	2009-01-15 00:00:00	31.0, 11043.0
Lauder	Radiosonde RS92 Vaisala	2009-01-21 09:51:00	370.0, 22274.0
Lamont	Radiosonde SGPCCP RS92-KL Vaisala	2009-01-29 17:27:00	315.0, 26242.6
Lamont	Radiosonde SGPCCP RS92-KL Vaisala	2009-01-30 17:30:00	315.0, 21694.0
Lamont	Radiosonde SGPCCP RS92-KL Vaisala	2009-01-31 17:28:00	315.0, 27814.4
Lamont	Radiosonde SGPCCP RS92-KL Vaisala	2009-02-01 17:31:00	315.0, 25996.2
Lamont	Radiosonde SGPCCP RS92-KL Vaisala	2009-02-04 17:29:00	315.0, 25760.4
Lamont	Radiosonde SGPCCP RS92-KL Vaisala	2009-02-05 17:29:00	315.0, 28314.8
Lamont	Radiosonde SGPCCP RS92-KL Vaisala	2009-02-07 17:30:00	315.0, 29041.6
Lamont	Radiosonde SGPCCP RS92-KL Vaisala	2009-07-22 17:30:00	315.0, 28323.9
Lamont	Radiosonde SGPCCP RS92-KL Vaisala	2009-07-23 17:34:00	315.0, 26027.4
Lamont	Radiosonde SGPCCP RS92-KL Vaisala	2009-07-24 17:29:00	315.0, 28031.9
Lamont	Radiosonde SGPCCP RS92-KL Vaisala	2009-07-28 17:40:00	315.0, 24764.1
Lamont	Radiosonde SGPCCP RS92-KL Vaisala	2009-07-30 17:26:00	315.0, 27132.0
Lamont	Radiosonde SGPCCP RS92-KL Vaisala	2009-07-31 17:30:00	315.0, 26045.4
Lamont	Radiosonde SGPCCP RS92-KL Vaisala	2009-08-02 16:02:00	315.0, 22369.1
Lamont	Radiosonde SGPCCP RS92-KL Vaisala	2009-08-03 17:28:00	315.0, 25592.3
Lamont	Radiosonde SGPCCP RS92-KL Vaisala	2009-08-05 17:28:00	315.0, 26822.7
Lamont	Radiosonde SGPCCP RS92-KL Vaisala	2009-08-07 17:29:00	315.0, 26150.3
Lamont	Radiosonde SGPCCP RS92-KL Vaisala	2009-08-08 17:27:00	315.0, 27160.1
Lamont	Radiosonde SGPCCP RS92-KL Vaisala	2009-08-09 17:32:00	315.0, 26842.1
Lamont	Radiosonde SGPCCP RS92-KL Vaisala	2009-08-12 17:29:00	315.0, 28095.5
Lamont	Radiosonde SGPCCP RS92-KL Vaisala	2009-08-13 17:30:00	315.0, 26099.5
Lamont	Radiosonde SGPCCP RS92-KL Vaisala	2009-08-14 17:28:00	315.0, 28220.8
Lamont	Radiosonde SGPCCP RS92-KL Vaisala	2009-08-15 17:30:00	315.0, 26032.9